Chapter 6: Titan's Atmospheric Structure, Composition, Haze, and Dynamics

Véronique Vuitton, Panayotis Lavvas, Conor A. Nixon, Nicholas A Teanby

▶ **To cite this version:**

Véronique Vuitton, Panayotis Lavvas, Conor A. Nixon, Nicholas A Teanby. Chapter 6: Titan's Atmospheric Structure, Composition, Haze, and Dynamics. Rosaly M.C. Lopes, Charles Elachi, Ingo Mueller-Wodarg, Anezina Solomonidou. Titan After Cassini-Huygens, Elsevier, 2024, 9780323991612. hal-04651963

HAL Id: hal-04651963
https://hal.science/hal-04651963v1

Submitted on 19 Jul 2024

HAL is a multi-disciplinary open access archive for the deposit and dissemination of scientific research documents, whether they are published or not. The documents may come from teaching and research institutions in France or abroad, or from public or private research centers.

L'archive ouverte pluridisciplinaire **HAL**, est destinée au dépôt et à la diffusion de documents scientifiques de niveau recherche, publiés ou non, émanant des établissements d'enseignement et de recherche français ou étrangers, des laboratoires publics ou privés.

Chapter 6: Titan's Atmospheric Structure, Composition, Haze, and Dynamics.

Véronique Vuitton[1], Panayotis Lavvas[2], Conor A. Nixon[3], and Nicholas A. Teanby[4]

[1]Univ. Grenoble Alpes, CNRS, IPAG, 38000 Grenoble, France
[2]Groupe de Spectrométrie Moleculaire et Atmosphérique, Université de Reims Champagne Ardenne, Reims, France
[3]Solar System Exploration Division, NASA Goddard Space Flight Center, Greenbelt, MD 20771, USA
[4]School of Earth Sciences, University of Bristol, Bristol, UK

July 21, 2023

1 Introduction

The Voyager flybys first revealed Titan's rich atmospheric organic inventory (Owen, 1982), which was confirmed beyond expectations by the Cassini-Huygens mission (Hörst, 2017). These observations triggered enormous modeling efforts over the last decades. The latest photochemical models include thousands of photochemical reactions coupling neutral and ion chemistry in order to reproduce the abundance of trace gas phase compounds observed throughout Titan's atmosphere. With the aid of microphysical models, processes leading to the formation and growth of organic aerosols have been explored. Finally, General Circulation Models (GCM) predict stratospheric temperatures and winds. Titan's chemical complexity has also inspired many to simulate these conditions in the laboratory. The complex organic compounds resulting from photolysis or radiolysis of N_2/CH_4 mixtures have been dubbed "tholins" and numerous studies have attempted to characterize their properties (Cable et al., 2012).

The goal of this Chapter is to give a description of Titan's basic vertical structure, composition and dynamics that is consistent with the constraints provided by the Cassini-Huygens mission and recent ground-based observations. We discuss the atmospheric mass, pressure and temperature, and radiative budget. We present the gas phase composition, from major constituents and inert gases to minor constituents and isotopes including neutral and charged species. We discuss the organic chemistry at the origin of this complex inventory. We review the size, shape, optical properties and vertical distribution of the photochemical haze and present our understanding of its formation and life cycle. We also discuss the presence, location and variations in condensation clouds over Titan's disk. We present the atmospheric dynamics in the stratosphere and mesosphere, including zonal winds, meridional circulation, and polar vortices. Finally, we indicate the prospects for further progress in understanding Titan's atmosphere in the future.

2 Main Vertical Structure

The Huygens probe descended through Titan's atmosphere on 14^{th} Jan 2005, landing at 10°S, 168°E, supplying a wealth of unique in-situ constraints (Lebreton et al., 2005). The Huygens Atmospheric Structure Instrument (HASI) measured a surface temperature of 93.7 K and a surface pressure of 1.467 bar at the landing site (Fulchignoni et al., 2005). Given Titan's low surface gravity of 1.35 m s^{-2}, a pressure this large indicates a significant atmospheric mass. A simple estimate of atmospheric mass M can be derived from the surface pressure p_0, body radius r, and gravity g: $M = 4\pi r^2 p_0/g$, assuming gravity does not vary with altitude, which is only approximate in Titan's case due to the extended nature of the atmosphere. This gives the mass of Titan's atmosphere to be approximately 9.1×10^{18} kg, almost twice that of the Earth's atmosphere at 5.2×10^{18} kg. An impressive amount of gas for such a small body.

A snapshot of Titan's temperature-pressure-altitude profile was also measured by HASI (Fulchignoni et al., 2005) (Figure 1). For Titan's equatorial region, the Huygens profile shows the tropopause occurs at ∼100 mbar/50 km, the stratopause at ∼10 μbar/250 km, and the mesopause at ∼1 μbar/500 km. However, there is significant variation in the profile with both latitude and season, as evidenced by the large variation in middle atmosphere temperature profiles measured by Cassini Composite InfraRed Spectrometer (CIRS) throughout the mission (Achterberg et al., 2011; Teanby et al., 2019; Vinatier et al., 2020) and subsequently from ground-based observations by the Atacama Large Millimeter/submillimeter Array (ALMA) (Lellouch et al., 2019; Thelen et al., 2022).

Titan's atmospheric temperature structure is remarkably similar to the Earth's, with a hot middle-atmosphere (stratosphere and mesosphere) indicating direct heating by solar radiation, although Titan's altitude scale is much more extended due to the lower gravity. On Earth the main middle-atmosphere solar absorbers are ozone and oxygen, but in Titan's reducing atmosphere absorption is more likely to be due to photochemical haze, methane, or trace gases. The similarities in temperature structure with Earth are one reason why Titan is so valuable for testing our understanding of atmospheric processes. Mars and Venus do not have significant middle-atmosphere absorption and so have very different temperature structures.

Up to the mesopause the temperature profile is similar to the pre-mission engineering temperature profile, based on Voyager radio science, Infrared Interferometer Radiometer Spectrometer (IRIS), and Ultraviolet Spectrometer (UVS) observations (Yelle et al., 1997). However, at higher altitudes (>500 km) there is significant structure, which could be due to atmospheric gravity waves or gravitational tides (Fulchignoni et al., 2005; Strobel, 2006; Muller-Wodarg et al., 2006). A careful analysis of the Huygens stratospheric temperature measurements also reveals that more subtle atmospheric waves exist there too (Lorenz et al., 2014). Gravity waves could be generated in the troposphere (see Chapter 8) and propagate upwards through the atmosphere, where they are amplified exponentially, due to reducing pressure, and become more easily visible. These waves may contribute to the atmospheric circulation and energy budget (Teanby et al., 2008; Strobel, 2006).

Energy sources in the upper atmosphere include solar radiation, photoelectrons and Saturnian magnetospheric electrons. The main energy source is solar extreme ultraviolet (EUV) and ultraviolet (UV) radiation, followed in importance by photoelectrons (produced by solar X-ray and EUV radiation) (Lavvas et al., 2011a). Saturnian magnetospheric electrons are dominant on the nightside of Titan but their contribution is always much lower than solar radiation on the dayside (Ågren et al., 2009; Galand et al., 2010). Energetic protons and

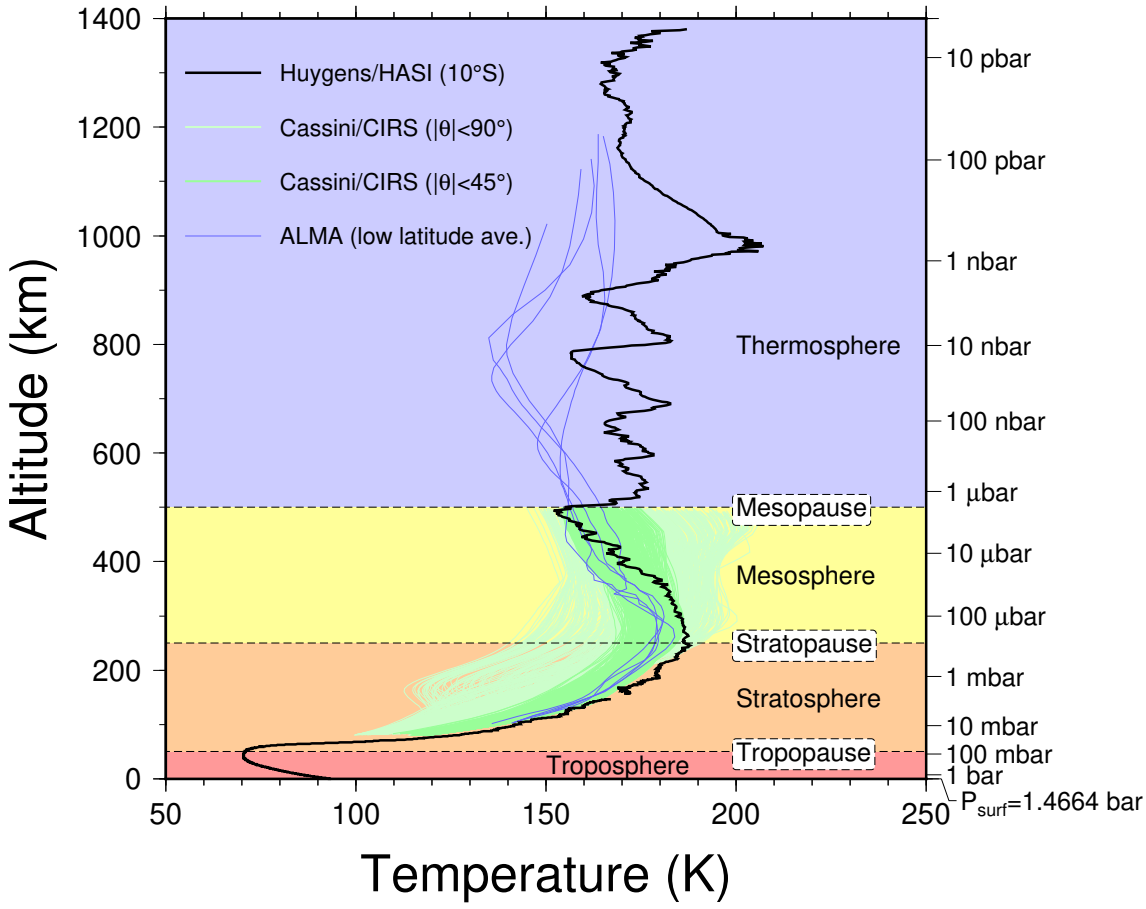

Figure 1: Titan's atmospheric temperature profile. The Huygens temperature profile was measured on 14$^{\text{th}}$ January 2005 at 10°S latitude. However, the temperature profile varies considerably with season and latitude θ, as illustrated by the Cassini Composite InfraRed Spectrometer (CIRS) middle atmosphere temperature profiles from Teanby et al. (2019) and the Atacama Large Millimeter/submillimeter Array (ALMA) profiles from Lellouch et al. (2019) and Thelen et al. (2022). Above the mesopause the Huygens measurements suggest there is wave activity in the thermosphere, but such features are not resolvable in the lower vertical resolution ALMA observations.

oxygen ions can also ionize the neutral species between 1000 and 500 km altitude but their contribution to the total ionization is small under typical conditions (Cravens et al., 2008). Nevertheless, oxygen ions are likely an important source of oxygen for Titan's atmosphere as discussed below (Hörst et al., 2008; Dobrijevic et al., 2014). Meteors ablate in the altitude range 800–600 km and create long-lived metallic ions but this represents a weak source of ionization overall (Molina-Cuberos et al., 2001). Galactic cosmic rays (GCR), due to their high energy, penetrate deep in the atmosphere where they generate some ionization with a peak contribution around 65 km and a magnitude comparable to ionization by solar photons in the upper atmosphere (Gronoff et al., 2009). Major energy sources are illustrated in Figure 1 of Chapter 3.

Measurements of Titan's emitted infra-red flux by Cassini/CIRS, combined with inferred sunlight absorption in the UV to near-infrared range from Cassini Imaging Science Subsystem (ISS) images, show that Titan's atmosphere is in approximate balance with absorbed solar radiation (Li et al., 2011; García Muñoz et al., 2017). This suggests it should be possible to explain Titan's temperature profile using radiative equilibrium. To test this, Bézard et al. (2018) developed a radiative-dynamical model of the equatorial atmosphere, where solar heating is balanced by radiative emission and adiabatic cooling from upwelling and the resulting expansion of air parcels. The model could match the observed temperature profile well if a slow upward vertical velocity of 0.3–0.5 $\mathrm{mm\,s^{-1}}$ at the 1 mbar level was included to provide adiabatic cooling in addition to radiative cooling. This adiabatic cooling was especially important for matching mesospheric temperatures, which were otherwise too warm. The model showed that for equatorial regions the main heating sources in Titan's middle atmosphere are solar absorption by methane and aerosols, and that the main cooling mechanism is emission by ethane, acetylene, methane, and aerosol (Bézard et al., 2018). The relative importance of different coolers changes significantly with latitude, especially for polar regions where there are significant enhancements of many radiatively active trace gases (Teanby et al., 2017).

3 Atmospheric Composition

3.1 Major Constituents and Inert Gases

It has been known since the time of the Voyager 1 encounter that Titan's atmosphere is mostly composed of molecular nitrogen (N_2) and methane (CH_4), with significant amounts of molecular hydrogen (H_2) and carbon monoxide (CO) (Broadfoot et al., 1981; Samuelson et al., 1981; Lutz et al., 1983). Molecular nitrogen is thought most likely to be a photolysis product from outgassed ammonia, accreted at the time of Titan's formation, while methane is being continuously or episodically replenished from the interior (Atreya et al., 1978; Tobie et al., 2006, and see also Chapter 3). Both H_2 and CO are secondary species, products of methane photolysis. This liberates hydrogen and carbon, some fraction of which reacts with externally supplied OH and O^+ to produce CO, CO_2 and H_2O (Hörst et al., 2008; Dobrijevic et al., 2014; Vuitton et al., 2019) - molecules that are all present in Titan's atmosphere (de Kok et al., 2007a; Coustenis et al., 1998; Moreno et al., 2012; Cottini et al., 2012; Serigano et al., 2016, and see Section 3.2). Measured volume mixing ratios (VMRs) of N_2 ($\sim$ 95–98%), CH_4 ($\sim$ 5–2%), H_2 ($\sim$ 0.1%) and CO ($\sim$50 ppm) in Titan's atmosphere are shown in Fig. 2.

The abundance of methane in Titan's atmosphere remains both highly important, but also uncertain in the details. It appears certain that the methane VMR decreases rapidly through

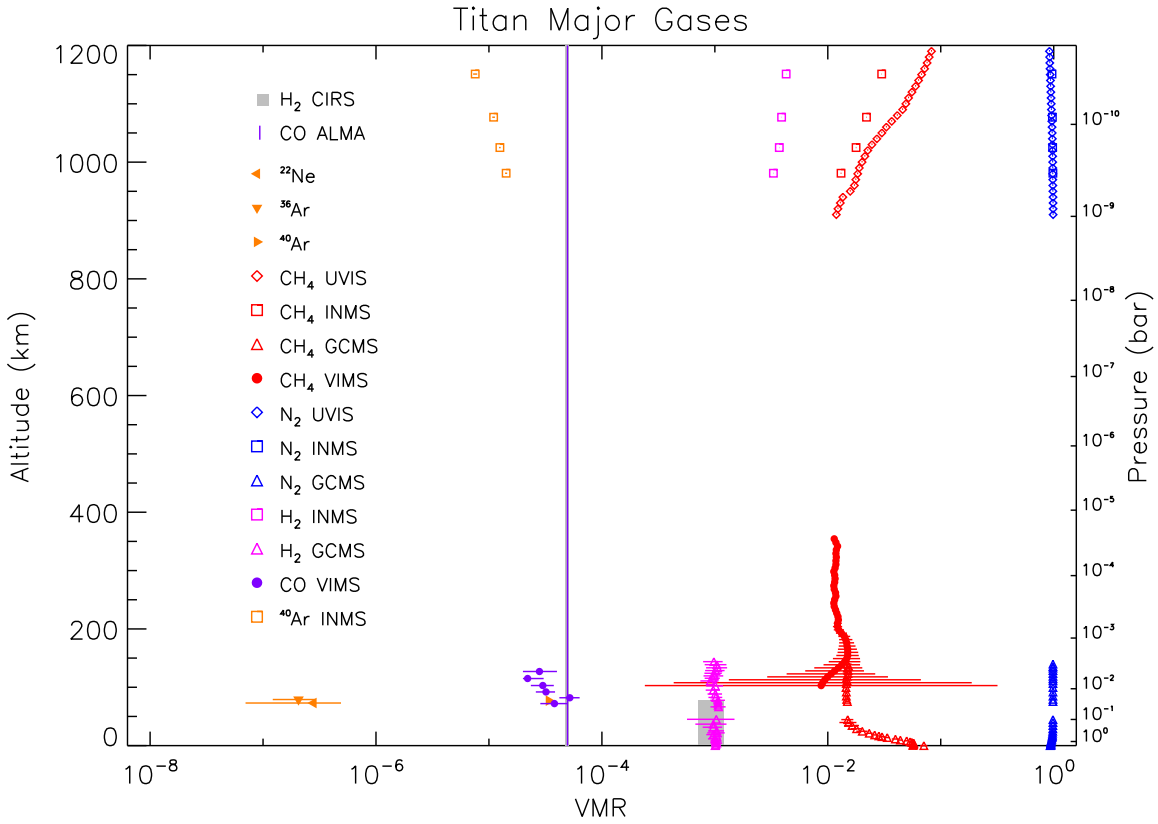

Figure 2: Volume mixing ratios for major species in Titan's atmosphere (N_2, CH_4, H_2, CO) and noble gases (^{22}Ne, ^{36}Ar, ^{40}Ar) as measured by Cassini-Huygens instruments and ALMA. Triangles: Huygens GCMS (Niemann et al., 2010) at 10°S. Diamonds: UVIS from Yelle et al. (2021) (ϵ-Orionis occultation). Squares: Cassini INMS (Cui et al., 2009b). Circles: Cassini VIMS (Rannou et al., 2022) (T53, 1°N). Grey shaded box: Cassini CIRS (Courtin et al., 2012). Purple line: ALMA (Serigano et al., 2016).

the troposphere, from a surface value of ∼5.5%, through to at least the tropopause (45 km, ∼100 mbar). This decrease is caused by the falling temperatures in this part of the atmosphere, contraining methane to its saturation humidity. The Huygens Gas Chromatograph Mass Spectrometer (GCMS) measurements showed a minimum VMRS of ∼ 1.48% at 45 km, and then a relatively constant mixing fraction upwards through the stratosphere (Niemann et al., 2010).

However, since the Huygens GCMS measurements were published, evidence has emerged for both vertical and latitudinal variation in the methane abundance. In 2014, analysis of methane rotational and vibrational bands measured by Cassini CIRS in the mid and far-IR indicated a latitudinal variation in the methane VMR at around 85 km altitude in the lower stratosphere, ranging from ∼1.0% at low latitudes and around ±50-55°, to a higher value of ∼1.5% at ±30-35° and at polar latitudes (Lellouch et al., 2014).

Analysis of near-IR solar occultation data from Cassini VIMS, where methane is seen in absorption, has been used to measure the methane profile from ∼100-400 km at various latitudes (Bellucci et al., 2009; Maltagliati et al., 2015). The most recent analysis (Rannou et al., 2022) shows evidence for a maximum VMR at 150-200 km (varying with latitude), with values decreasing above and below. At the equator, the stratospheric maximum VMR was ∼1.5% at ∼150 km, decreasing upwards and then stabilizing at ∼1.2% above 200 km. The authors suggest that these variations may be linked to stratospheric circulation, re-distributing methane on a global scale.

Further data on methane's vertical profile was provided by the Upward Looking Infrared Spectrometer (ULIS), part of the Huygens' DISR instrument (Tomasko et al., 2003), also sensitive to near-IR absorption. Interpretation of this data has been hampered due to uncertainties in the methane line parameters in the near-IR, especially the crucial 1.4 μm band. While the initial analysis of Bézard (2014) showed an abundance of 1.44 (+0.27/-0.11) % in the lower stratosphere, consistent with Huygens GCMS, a later re-analysis by Rey et al. (2018) using an updated spectroscopic line model indicated a decreasing profile in the lower stratosphere, reaching ∼1% at 110 km.

At higher altitudes, in the thermosphere, the methane homopause is reached at ∼900 km and its vertical scale height decouples from that of N_2 (Bell et al., 2011). At this point, its VMR begins to rise again, although substantial variability is seen (De La Haye et al., 2007; Cui et al., 2009a; Magee et al., 2009).

The VMR of molecular hydrogen has proved contentious, with a value 4× higher in the ionosphere (0.33-0.43%) (Waite et al., 2005; Cui et al., 2009b) than the troposphere and stratosphere (∼0.1%) (Niemann et al., 2010; Courtin et al., 2012; Bézard and Vinatier, 2020). This implied a large sink for hydrogen at the surface, incompatible with any currently devised model (Strobel, 2010). A possible solution to this puzzle has recently been postulated by Strobel (2022), who suggests that an error in the calibration of the INMS data may have led to an over-estimation of the ionospheric H_2 by a factor of 2.2, which if true would allow the VMR to be revised downwards to a value compatible with current models.

Carbon monoxide is thought to be well-mixed in Titan's atmosphere, with a constant abundance throughout, due to its long photochemical lifetime (∼500 Myr, Vuitton et al., 2019) and its molecular mass being almost identical to the bulk atmospheric constituent (N_2). However, its mass similarity to N_2 also makes it difficult to measure with low resolution mass spectrometry techniques (i.e. INMS, GCMS), so only remote sensing measurements exist from CIRS and ground-based astronomy (de Kok et al., 2007a; Teanby et al., 2010b;

Serigano et al., 2016).

Three inert (noble) gas isotopes have been measured in Titan's atmosphere. The Huygens GCMS descent measurements detected ^{36}Ar and ^{40}Ar, and tentatively ^{22}Ne (Niemann et al., 2010), while the Cassini INMS measured ^{40}Ar in the upper atmosphere (Cui et al., 2009b) (see Fig. 2). ^{36}Ar is a primordial species, and its presence at a low level is expected from accretion from the solar nebula. However the ratio of ^{14}N/^{36}Ar $\sim 1\times10^7$ is substantially larger than on Earth and Mars ($\sim 4 \times 10^4$) (Niemann et al., 2010) and implies that Titan formed at a warmer temperature than the inner planets (Owen and Niemann, 2009). On the other hand, the presence of the radiogenic isotope ^{40}Ar (produced by beta decay of ^{40}K) implies significant outgassing over Titan's history, although comparatively less than the Earth's activity (Niemann et al., 2010). The presence of ^{22}Ne requires some careful modeling to explain, since the gas is difficult to trap except at extremely cold temperatures (Niemann et al., 2010). Finally, Kr and Xe were not detected by GCMS, with upper limits of 10 ppb (Niemann et al., 2010), although this is unsurprising since the instrument was not expected to detect these gases, expected at levels < 1 ppb (Owen and Niemann, 2009).

3.2 Minor Constituents

Cassini's Ion Neutral Mass Spectrometer and Plasma Spectrometer (INMS and CAPS) performed the first and only in-situ density measurements during low altitude passes through Titan's upper atmosphere. An example of the positive ion mass spectrum for a mass range of m/z = 1–100 extracted from INMS data is given in Figure 3. Some obvious features are immediately seen. First, there are more than 50 mass channels with a density higher than 0.1 cm^{-3}. No unique ion species dominates Titan's ionosphere, in contrast to the neutral gas distribution for which N_2 has a mixing ratio of over 95% (Waite et al., 2005; Vuitton et al., 2007). Furthermore, measurements from the CAPS Ion Beam Spectrometer (IBS) revealed positive ions up to m/z = 350 (Waite et al., 2007; Crary et al., 2009). The right panel of Figure 4 shows an example of IBS spectrum. Positive ion spectra are characterized by distinct mass groups with a mean mass spacing of m/z = 12–14, characteristic of organic compounds with a carbon backbone (Cravens et al., 2006; Haythornthwaite et al., 2021).

Although it was designed to detect electrons, CAPS Electron Spectrometer (ELS) showed evidence for negatively charged ions with a mass-to-charge ratio reaching up to m/z ∼14,000, including three distinct low mass peaks at m/z = 25.8–26.0, 49.0–50.1 and 71–94 (Coates et al., 2007; Desai et al., 2017). These low-mass negative ions present lower densities on the night side and increased densities up to twice as high on the day side at small solar zenith angles (Mihailescu et al., 2020). The left panel of Figure 4 shows an example of ELS spectrum.

INMS detected the neutrals C_2H_2, C_2H_4,C_2H_6,C_3H_4,C_4H_2,C_6H_6, HC_3N and C_2N_2 around 1000 km. NH_3 has been detected by INMS as well but it remains unclear if it is actually a product of atmospheric chemistry, of the reaction of N and H on the instrument chamber walls or of spent hydrazine.

Analysis of the mass spectrometry data was limited by the instruments low mass resolution that prevented resolving isobaric neutral and ion species. Moreover, while CAPS-IBS densities are scaled to the INMS densities, CAPS-ELS densities are only approximate because the efficiency of the microchannel plates was never tested for negative ions and it could be underestimated by one order of magnitude (Mihailescu et al., 2020).

Besides direct mass spectrometry, information on the profiles of minor gases has come

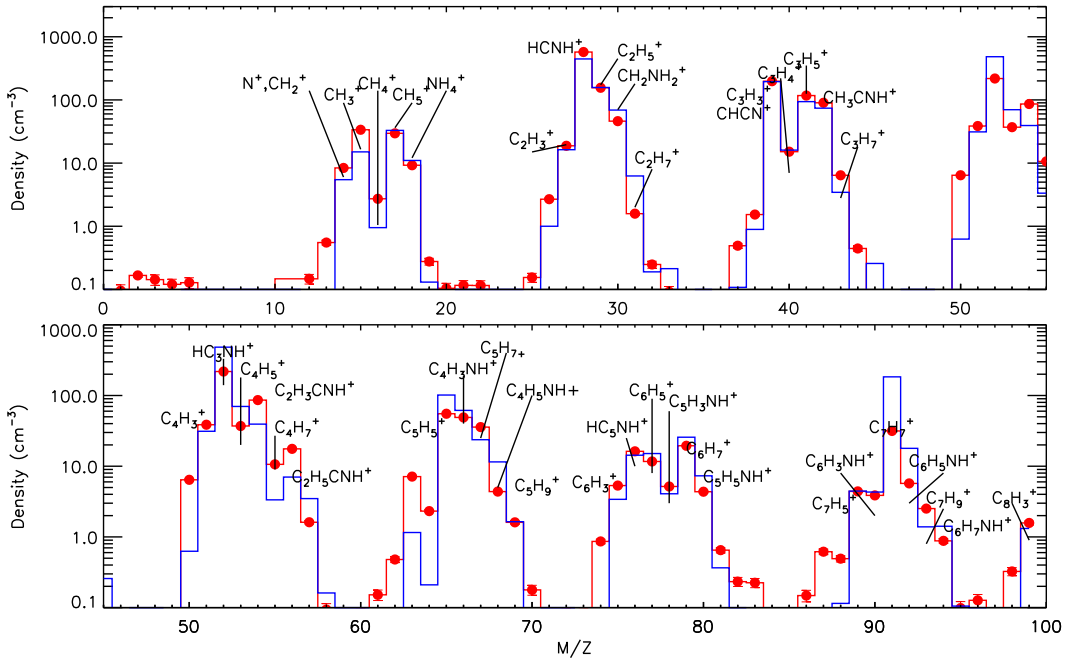

Figure 3: Cassini/INMS (dots connected by red lines) and computed (blue lines) mass spectrum at 1100 km. Reproduced from Vuitton et al. (2019).

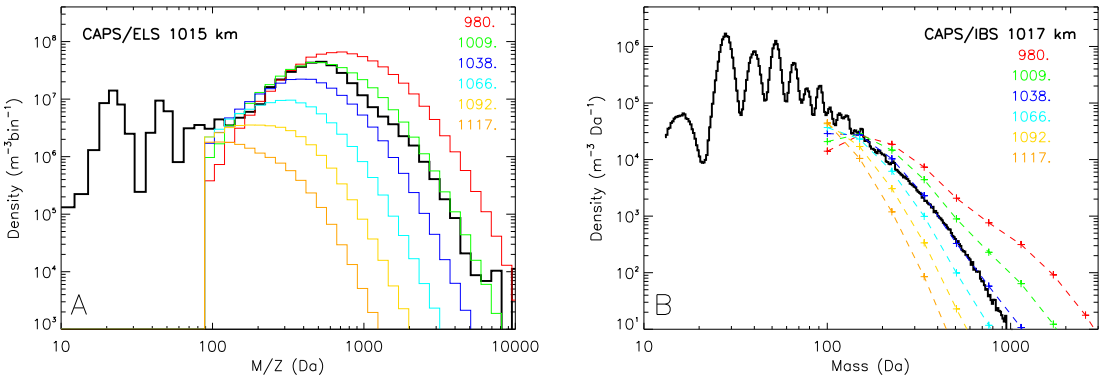

Figure 4: Observed and simulated mass/charge distributions of large mass negative (A) and positive (B) in Titan's ionosphere (from Lavvas et al., 2013). Black lines present the measured distributions near 1000 km while coloured lines the simulated evolution of the mass/charge distribution with altitude.

from remote sensing measurements by Cassini's UVIS (Fan et al., 2019; Yelle et al., 2021), VIMS (Maltagliati et al., 2015), and CIRS (Cottini et al., 2012; Lombardo et al., 2019a; Mathé et al., 2020) instruments, as well as ground-based observatories - especially IRTF/TEXES and ALMA (Cordiner et al., 2014; Cordiner et al., 2015; Palmer et al., 2017; Lellouch et al., 2019; Lombardo et al., 2019b; Thelen et al., 2019; Nixon et al., 2020; Thelen et al., 2020).

Figure 5 shows CIRS limb spectra covering the 100–300 km stratospheric range for equatorial and south polar regions during southern winter, indicating multiple trace gas and condensate features throughout the far- and mid-IR. Such spectra have been used extensively to measure trace gas profiles (e.g. Teanby et al., 2017; Mathé et al., 2020; Vinatier et al., 2020). Figure 6 shows typical low-latitude or disk-averaged gas profiles. In general, trace gases show profiles that are decreasing downwards (with increasing pressure), due to the molecules being created in the upper atmosphere and then diffusing downwards into steadily increasing amounts of background atmosphere and for most minor species, a lower stratosphere condensation sink. The profiles are more constant however in winter polar regions due to more rapid subsidence and dynamical mixing, as discussed in Section 6.2. The mixing ratio decreases with the complexity of the molecule as would be expected and, for a given number of C-atoms, saturated species are more abundant than unsaturated ones.

Besides detected species, upper limits have been obtained by various techniques for undetected species - upper limits for the neutral atmosphere from remote sensing measurements are given in Table 1. Remote sensing detection of increasingly large molecules by their IR ro-vibrational bands becomes challenging for three reasons: (a) lower abundances, due to lower production rates, and lower vapor pressures; (b) larger numbers of infrared bands per molecule in which to spread thermal emission (Nixon et al., 2009); (c) greater numbers of isomers, including conformers, with unique bands. Sub-millimeter detection of rotational lines has some advantages and disadvantages over IR detection: it is generally sensitive to lower abundances and temperatures, however it is limited to asymmetric molecules that have a dipole moment, whereas IR spectroscopy can in principle detect all molecules.

3.3 Isotopes

To date, five 'stable' isotopic ratios have been measured in Titan's atmosphere: D/H, $^{12}C/^{13}C$, $^{14}N/^{15}N$, $^{16}O/^{18}O$, $^{16}O/^{17}O$ - spread amongst eleven molecular species. Numerous measurements have been made by a variety of in-situ and remote sensing techniques (mass spectrometry, infrared and sub-millimeter spectroscopy), with some of the most recent summarized in Table 2.

Deuterium is strongly partitioned from nebular hydrogen gas (H_2) to ices (CH_4, NH_3, H_2O etc) (Mousis et al., 2002; Mousis et al., 2002). This can clearly be seen by comparing the low D/H values seen in H_2 in Jupiter and Saturn ($2 - 3 \times 10^{-5}$, Pierel et al., 2017) to the much higher values seen in comets ($\sim 20 - 50 \times 10^{-5}$, Bockelée-Morvan et al., 2015). The intermediate value seen in Titan's methane (13×10^{-5}, Bézard et al., 2007), similar to the Earth Standard D/H (VSMOW, 15.6×10^{-5}), may indicate a similar origin of volatile materials, possibly the Jupiter Family Comets or Kuiper Belt Objects (Hartogh et al., 2011). On the other hand, the apparent D/H enrichment seen in Titan's C_2H_2 and HCN compared to D/H in methane may be evidence for a kinetic isotope effect (Nixon et al., 2012) that is enriching D/H in daughter products due to preferential photolysis/abstraction and subsequent escape of ^1H.

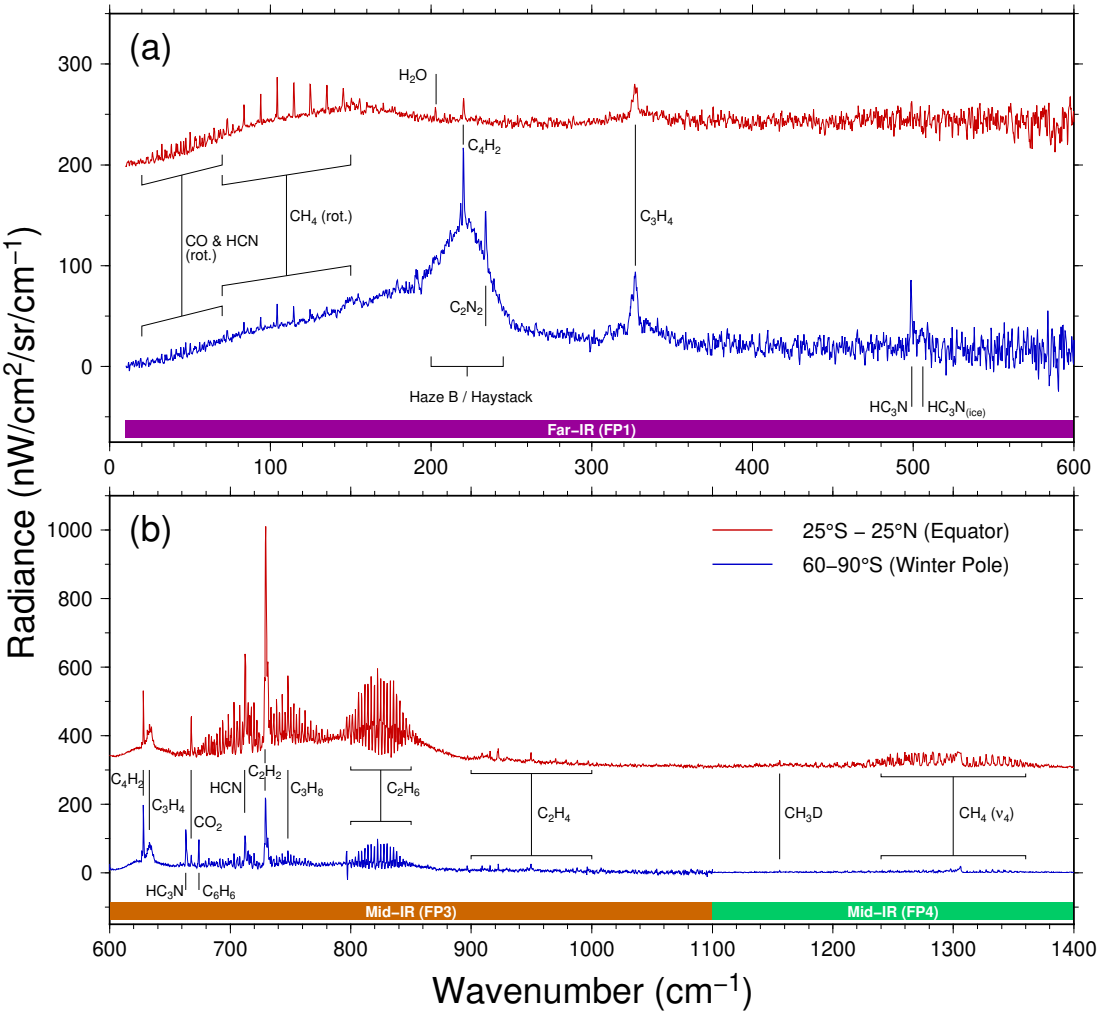

Figure 5: Cassini/CIRS limb spectra for the 100–300 km tangent altitude range for the southern winter season. Multiple CIRS observations between 2012–2015 have been averaged together to improve signal-to-noise for the south pole and equatorial regions (e.g. Teanby et al., 2017; Mathé et al., 2020; Vinatier et al., 2020). The equatorial limb spectra (red) is typical of those observed throughout the mission and shows emission features from minor hydrocarbon and nitrile species. The south polar spectrum (blue) is when trace species were greatly enhanced and stratospheric temperatures were a lot colder than equatorial region because of additional radiative cooling. The cold temperatures are evident as reduced emission in the CH_4 (ν_4) band at $\sim$1300 cm^{-1} (panel b), whereas winter enhancement of trace species is indicated by additional emission features from HC_3N and C_6H_6 (panels a and b), whose abundances are too low at equatorial latitudes to give an obvious emission feature. Additionally, the Haze B/Haystack condensate feature and HC_3N ice are also visible (panel a), which are only seen at the winter pole.

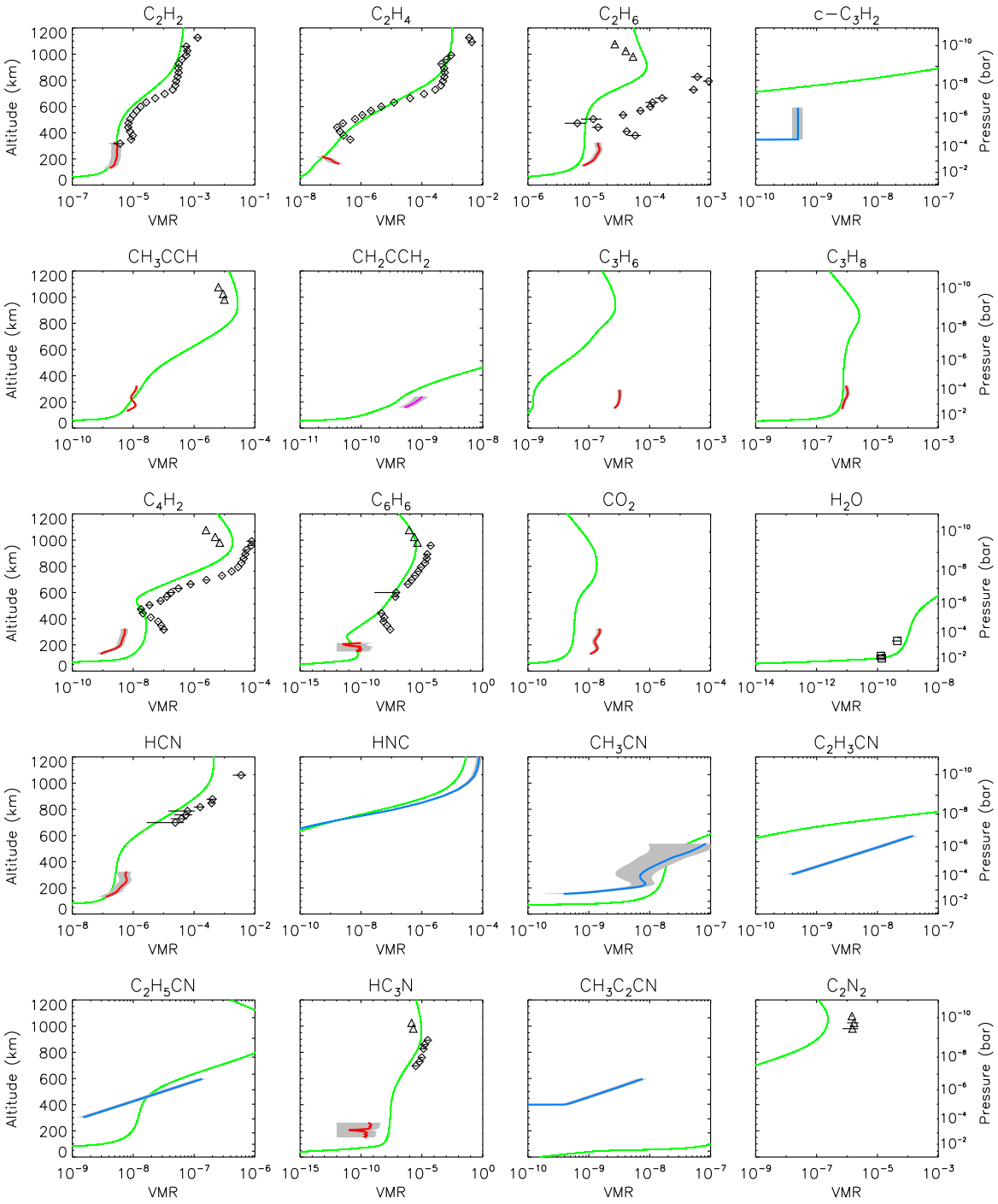

Figure 6: Profiles of minor gases in Titan's atmosphere. Triangles: INMS from Cui et al. (2009b). Diamonds: UVIS FUV measurements from Yelle et al. (2021) (HCN: ζ-Orionis occultation, other gases: ϵ-Orionis occultation). Squares: CIRS from Cottini et al. (2012). Red lines: CIRS from Mathé et al. (2020) except C_3H_6 from Lombardo et al. (2019a). Magenta line: CH_2CCH_2 from IRTF/TEXES Lombardo et al. (2019b). Blue lines, ALMA: HNC - Lellouch et al. (2019); CH_3CN - Thelen et al. (2019); C_2H_5CN - Cordiner et al. (2015); C_2H_3CN - Palmer et al. (2017); CH_3C_3N - Thelen et al. (2020); C_3H_2 - Nixon et al. (2020). Green lines: model profiles from Vuitton et al. (2019).

Species	Instrument	Altitude or Pressure	VMR (ppbv)	Reference
		Hydrides and Diatomic		
NH_3	CIRS	0.27 mbar	< 0.59 (1σ)	Nixon et al. (2010)
NH_3	SPIRE	75 km	< 0.19 (3σ)	Teanby et al. (2013)
SH_2	CIRS	0.27 mbar	< 91 (1σ)	Nixon et al. (2013)
PH_3	CIRS	0.27 mbar	< 0.30 (1σ)	Nixon et al. (2013)
CS	ALMA	> 200 km	< 0.0256 (3σ)	Teanby et al. (2018)
		Hydrocarbons		
i-C_4H_{10}	CIRS	225 km	< 39 (1σ)	Hewett et al. (2020)
n-C_4H_{10}	CIRS	272 km	< 177 (1σ)	Steffens et al. (2022)
C_6H_2	IRIS	100 km	< 6.5 (1σ)	Khlifi et al. (1996)
		Nitriles X-CN		
$CH_3(CH)_2CN$	ISO	150 km	< 0.5 (1σ)	Coustenis et al. (2003)
CH_2CHCH_2CN	ISO	150 km	< 0.5 (1σ)	Coustenis et al. (2003)
$CH_2C(CH_3)CN$	ISO	150 km	< 0.5 (1σ)	Coustenis et al. (2003)
n$-C_3H_7CN$	IRIS	100 km	< 10 (1σ)	Raulin (1990)
i$-C_3H_7CN$	IRIS	100 km	< 25 (1σ)	Raulin (1990)
c$-C_3H_5CN$	IRIS	100 km	< 0.5 (1σ)	Raulin (1990)
HC_5N	IRAM	> 80 km	< 0.40 (1σ)	Marten et al. (2002)
C_4N_2	CIRS	150 km	< 0.53 (1σ)	Jolly et al. (2015)
		Other Organic Nitrogen CNH		
CH_2N_2	IRIS	100 km	< 5.0 (1σ)	Khlifi et al. (1996)
CH_3N_3	IRIS	100 km	< 5.4 (1σ)	Khlifi et al. (1996)
CH_3NC	IRIS	100 km	< 1.3 (1σ)	Khlifi et al. (1996)
CH_2NH	ALMA	> 50 km	< 0.35 (3σ)	Teanby et al. (2018)
c$-C_5H_5N$	ALMA	$p < 0.10$ mbar	< 1.05 (1σ)	Nixon et al. (2020)
c$-C_4H_4N_2$	ALMA	$p < 0.10$ mbar	< 0.66 (1σ)	Nixon et al. (2020)
		Organic Oxygen Compounds CHO		
H_2CO	CIRS	0.27 mbar	< 2.20 (1σ)	Nixon et al. (2010)
CH_3OH	CIRS	0.27 mbar	< 6.40 (1σ)	Nixon et al. (2010)

Table 1: Upper limits for undetected trace species in Titan's stratosphere.

Ratio	Species	Instrument	Value	Reference
D/H	H_2	INMS	$(1.35 \pm 0.30) \times 10^{-4}$	Niemann et al. (2010)
D/H	CH_4	CIRS	$(1.32^{+0.15}_{-0.11}) \times 10^{-4}$	Bézard et al. (2007)
D/H	C_2H_2	CIRS	$(2.09 \pm 0.45) \times 10^{-4}$	Coustenis et al. (2008)
D/H	HCN	ALMA	$(2.5 \pm 0.2) \times 10^{-4}$	Molter et al. (2016)
$^{12}C/^{13}C$	CH_4	INMS	91.1 ± 1.4	Niemann et al. (2010)
$^{12}C/^{13}C$	C_2H_2	CIRS	84.8 ± 3.2	Nixon et al. (2008a)
$^{12}C/^{13}C$	C_2H_6	CIRS	89.8 ± 7.3	Nixon et al. (2008a)
$^{12}C/^{13}C$	C_4H_2	CIRS	90 ± 8	Jolly et al. (2010)
$^{12}C/^{13}C$	HCN	ALMA	89.8 ± 2.8	Molter et al. (2016)
$^{12}C/^{13}C$	HC_3N	CIRS	79 ± 17	Jennings et al. (2008)
$^{12}C/^{13}C$	CO	ALMA	89.9 ± 3.4	Serigano et al. (2016)
$^{12}C/^{13}C$	CO_2	CIRS	84 ± 17	Nixon et al. (2008b)
$^{14}N/^{15}N$	N_2	INMS	167.7 ± 0.6	Niemann et al. (2010)
$^{14}N/^{15}N$	HCN	ALMA	72.3 ± 2.2	Molter et al. (2016)
$^{14}N/^{15}N$	HC_3N	ALMA	67 ± 14	Cordiner et al. (2018)
$^{14}N/^{15}N$	CH_3CN	ALMA	125^{+145}_{-44}	Iino et al. (2020)
$^{16}O/^{17}O$	CO	ALMA	2917 ± 359	Serigano et al. (2016)
$^{16}O/^{18}O$	CO	ALMA	486 ± 22	Serigano et al. (2016)
$^{16}O/^{18}O$	CO_2	CIRS	380 ± 142	Nixon et al. (2008b)

Table 2: Selected recent measurements of isotopic ratios in Titan's atmosphere

While carbon $^{12}C/^{13}C$ and the oxygen isotope ratios $^{16}O/^{18}O$ and $^{16}O/^{17}O$ in all molecules show little discernible deviation from terrestrial or giant planet values, nitrogen $^{14}N/^{15}N$ on the other hand shows a large difference from the parent species N_2 to the daughter nitriles (HCN, HC_3N and CH_3CN). Nitrogen $^{14}N/^{15}N$ is lower in N_2 ($\sim$ 168, Niemann et al., 2010) than the Earth ($\sim$ 272, Anders and Grevesse, 1989) and dramatically lower than Jupiter (435, Wong et al., 2004), while the value in HCN is lower still (72, Molter et al., 2016).

Photochemical models are able to produce $HC^{14}N$/ $HC^{15}N$, $CH_3C^{14}N/CH_3C^{15}N$ and $HC_3{}^{14}N$/ $HC_3{}^{15}N$ ratios in reasonably good agreement with Cassini and ALMA observations (Dobrijevic and Loison, 2018; Vuitton et al., 2019). The difference in the $^{14}N/^{15}N$ between N_2 and trace nitriles is explained by the photolytic fractionation of N_2 and $^{14}N^{15}N$ induced by isotope-selective shielding. This shows how important it is to take into account the high resolution photodissociation cross sections of both N_2 and $^{14}N^{15}N$ to compute their photolysis rates (Liang et al., 2007; Lavvas et al., 2011a).

4 Gas Phase Atmospheric Chemistry

The complex organic inventory observed in-situ and with remote sensing instruments, as discussed in Section 3.2, demonstrates that Titan's atmospheric chemistry is diverse and complex.

Before this suite of constituents was discovered, Strobel (1974) developed the basic framework of methane photochemistry in Titan's atmosphere and concluded that, because of the high efficiency of hydrogen escape, it leads to irreversible loss of CH_4 on a time scale short compared to Titan's age (10s MY). Subsequently, numerous 1D photochemical models have been designed to explain the composition of Titan's atmospheric column (Dobrijevic et al., 2016; Vuitton et al., 2019). Chemistry is initiated by the ionization and dissociation of molecular nitrogen and methane by solar ultraviolet photons, suprathermal electrons (magnetospheric as well as photoelectrons and their secondaries) and GCR. The main primary species produced are N_2^+, N^+, $N(^2D)$, $N(^4S)$ and CH_3, $^1CH_2$, CH, CH_4^+, CH_3^+ (Lavvas et al., 2011a). They react with the background gas through a large network of thousands of ion-neutral and neutral-neutral chemical reactions to generate hundreds of positive and negative ions as well as neutral molecules (up to 7 heavy atoms). The efficiency and the products of these reactions depend on the background composition and on atmospheric pressure and temperature. In addition, the distribution of species is affected by molecular diffusion and dynamics, as well as the escape of the lightest compounds and the condensation of the heaviest ones in the lower stratosphere (see Section 5.2).

As inferred from these calculations, in most cases, a single ion species contributes to the INMS signal in a given channel, with only a small fraction (typically less than 10%) from other minor ions. The most abundant ions are closed-shell species because radical cations are not very stable and therefore react quickly. This implies that while odd mass channels are attributed to hydrocarbon ions, peaks at even m/z are the signature of ions containing one nitrogen atom. The most abundant ion species is $HCNH^+$, followed by $C_2H_5^+$, $c{-}C_3H_3^+$, HC_3NH^+ and $C_3H_5^+$. The high modeled abundance of $HCNH^+$ and $C_2H_5^+$ is consistent with experimental work simulating the primary steps of Titan's ionospheric chemistry (Thissen et al., 2009; Dubois et al., 2020). The ion species that account for channels with number densities greater than 1 cm^{-3} are labeled in Figure 3 for reference. Light ions are primarily lost through ion-neutral chemistry whereas heavy ions are primarily lost through electron recombination (Vuitton et al., 2006b, 2007). Qualitatively, the dayside and nightside positive ion compositions are similar, but quantitative differences exist, particularly for the species with relatively short chemical lifetimes (CH_5^+, $HCNH^+$, $C_2H_5^+$) that are more abundant on the dayside. On the other hand, the day-to-night variations for terminal ion species with long lifetimes (NH_4^+, $C_6H_7^+$, $C_2H_3CNH^+$) are rather small (Cui et al., 2009a). Although model results can mostly reproduce the INMS mass spectra, it remains difficult to interpret the signals at m/z 50, 64 and 74 (Vuitton et al., 2019). Another notable issue is that the observed total positive ion density (essentially $HCNH^+$ and $C_2H_5^+$) is systematically overestimated by a factor of 2–3. This discrepancy is related to the overproduction of electrons in dayside models, as discussed in Vigren et al. (2013) and Sagnières et al. (2015), and remains unexplained.

Models predict that CN^- is the dominant negative ion in Titan's ionosphere, followed by C_3N^-. H^- is also predicted as an abundant ion, especially at higher altitudes. CH_2^-, C_2H^-, C_4H^- and C_5N^- exhibit some significant abundances but their density profile is more model dependent (Vuitton et al., 2009; Dobrijevic et al., 2016; Mukundan and Bhardwaj, 2018; Vuitton et al., 2019). These predictions are in agreement with laboratory experiments where CN^-, C_3N^-, and C_5N^- were detected in N_2/CH_4(/Ar) dusty plasmas (Horvath et al., 2010; Dubois et al., 2019a). Noteworthy, a number of compounds containing two or three nitrogen atoms (e.g. CNN^-, $CHNN^-$) not considered in models are also observed in these experiments. The combination of m/z and relative density profile suggests that CN^- / C_3N^-(C_4H^-) /

C_5N^- (C_6H^-) are the anions that cause the peaks at 26 / 49–50.1 / 71–94 in the CAPS-ELS data. H^- cannot be measured by CAPS-ELS because of the spacecraft velocity (Desai et al., 2017). Negative ions are essentially formed by dissociative and radiative attachment of energetic and thermal electrons, respectively onto neutral species. This is in agreement with the low-mass negative ion density and the electron density measured by Cassini's Langmuir Probe to be proportional to each other on the day side but independent of each other on the night side (Mihailescu et al., 2020). Electron distributions depend on solar illumination conditions and magnetospheric configuration (Ågren et al., 2009; Galand et al., 2010), which probably explains at least some of the variability in density and altitude of the peaks observed in the CAPS-ELS data (e.g. Fig. 2 of Wellbrock et al. (2013)). Just as with positive ions, proton transfer reactions lead to the formation of heavier negative ions. Finally, negative ions are lost by associative detachment reactions with the most abundant radicals, typically H and CH_3. Models produce much fewer anions than suggested by the observations (Wellbrock et al., 2013), which may either be explained by a missing source of light negative ions in models or the uncertain efficiency of the CAPS-ELS microchannel plates (Mihailescu et al., 2020).

The production of the trace neutral species is mostly driven by neutral reactions. Nevertheless, the failure of pure neutral chemistry to reproduce the abundance of some species, especially in the upper atmosphere, is indicative of the interplay between ion and neutral trace constituents. While acetylene (C_2H_2), hydrogen cyanide (HCN) and other nitriles are exclusively formed by radical chemistry, benzene (C_6H_6), ammonia (NH_3), methanimine (CH_2NH) and hydrogen isocyanide (HNC) are affected by the coupled ion and neutral chemistry. These species are transported downward to the stratosphere where the photolysis of acetylene is indirectly responsible for the dissociation of methane, through catalytic processes (Vuitton et al., 2006a). Radical-radical association efficiently forms alkanes in the stratosphere including ethane (C_2H_6), the most abundant photochemical product. Model results are generally in agreement with observations for most neutral compounds in both thermosphere and stratosphere but some discrepancies remain for a few compounds, such as NH_3, HC_3N, C_2H_5CN, C_2N_2 (Dobrijevic et al., 2016; Vuitton et al., 2019). The overestimation of nitriles could be explained by their role in aerosol formation or their adsorption on the aerosol surface, processes that have been shown to happen in the laboratory (Imanaka and Smith, 2010; Couturier-Tamburelli et al., 2018a) but are not properly taken into account in photochemical models yet. Models having an upgraded reaction network involving benzene highlight its potential contribution in the formation of more complex aromatic compounds such as toluene ($C_6H_5CH_3$) and ethylbenzene ($C_6H_5C_2H_5$) (Loison et al., 2019). However, both aromatics have not been detected yet. Laboratory simulations that have been used to investigate the gas products formed in high-energy plasmas or ultraviolet irradiation of a CH_4/N_2 mixture emphasized the detection of ammonia, methanimine, benzene and toluene (e.g. Bourgalais et al. (2019); Dubois et al. (2019b); Bourgalais et al. (2021) and references therein). However, direct comparison of the results of these experiments with Titan should be performed with caution as temperature/pressure conditions and energy sources differ from Titan, and the formation of some species has been shown to be mainly driven by wall effects (Thissen et al., 2009). Nevertheless, in a series of experiments using FUV photons, Hörst et al. (2018) measured concentrations of small gas-phase species that are consistent with concentrations in Titan's stratosphere.

The HASI experiment onboard the Huygens probe measured a peak electron density of

$\sim$650 cm^{-3} at 65 km, which is attributed to ionization by GCR (Hamelin et al., 2007; López-Moreno et al., 2008; Gronoff et al., 2011). However, in photochemical models, the maximum of the GCR ionization peak is at 90 km, with a magnitude of $\sim$2000 cm^{-3} (Molina-Cuberos et al., 1999; Vuitton et al., 2019). It has been pointed out that models do not take into account electron attachment onto aerosols or electrophilic species, which could reduce the electron densities by significant factors and explain the discrepancy with the Huygens measurement (Borucki and Whitten, 2008; Molina-Cuberos et al., 2018). GCR induce the formation of nitrogen atoms and ions, which results into some increase of most nitrogen compounds (Lavvas et al., 2008; Loison et al., 2015; Vuitton et al., 2019). Although there are no observations that constrain the ion composition in Titan's stratosphere, Berry et al. (2019) observe in their laboratory simulations an extensive nitrogen incorporation into cations up to m/z 400, including ions with multiple nitrogen atoms, in agreement with the photochemical models predictions.

5 Haze and Ice Clouds

5.1 Photochemical haze

The instruments on board Cassini and Huygens permitted a panchromatic investigation of the photochemical haze properties in Titan's atmosphere (Fig. 7). In situ studies with the Cassini mass spectrometers in the upper atmosphere (above $\sim$900 km) in conjunction with remote sensing investigations from UV to IR wavelengths allowed for the study of haze formation and evolution. In addition, in situ measurements with instruments on board the Huygens probe revealed for the first time fundamental properties for the haze composition, structure, and optical properties. Here we overview these results starting from the haze embryo formation in the upper atmosphere and following its evolution through Titan's atmosphere.

5.1.1 Embryo formation in the ionosphere

The heavy negative ions observed with the CAPS instrument (Fig. 4) revealed that Titan's ionosphere is the birthplace of the observed photochemical haze (Waite et al., 2007; Coates et al., 2007). These haze embryos have increasing masses with decreasing altitude in the ionosphere, as well as with increasing geographical latitude, and appear to grow more efficiently during low illumination conditions, particularly those of the polar winter (Coates et al., 2009, 2010; Wellbrock et al., 2013, 2019). CAPS was not anticipated to act as a mass spectrometer thus was not designed with a sufficient resolution for precise identification of the molecular structures identified in positive and negative mode. Therefore, the interpretation of the observed mass/charge spectra is approximate, particularly for the large mass ions. Both aliphatic and aromatic compounds are expected to contribute to the observed distributions (Waite et al., 2007; Crary et al., 2009; Sittler et al., 2009; Desai et al., 2017), with the latter having a higher probability and including both PAH and nitrogen containing polyaromatic structures (Haythornthwaite et al., 2021). The presence of polyaromatic structures in the first steps of haze formation is further supported by the detection with VIMS of non-LTE molecular emissions in Titan's upper atmosphere at near IR wavelengths that were attributed to PAHs (Dinelli et al., 2013; López-Puertas et al., 2013). Laboratory simulations also show that tholins contain a trace amount of small PAHs with at least one aromatic ring, while

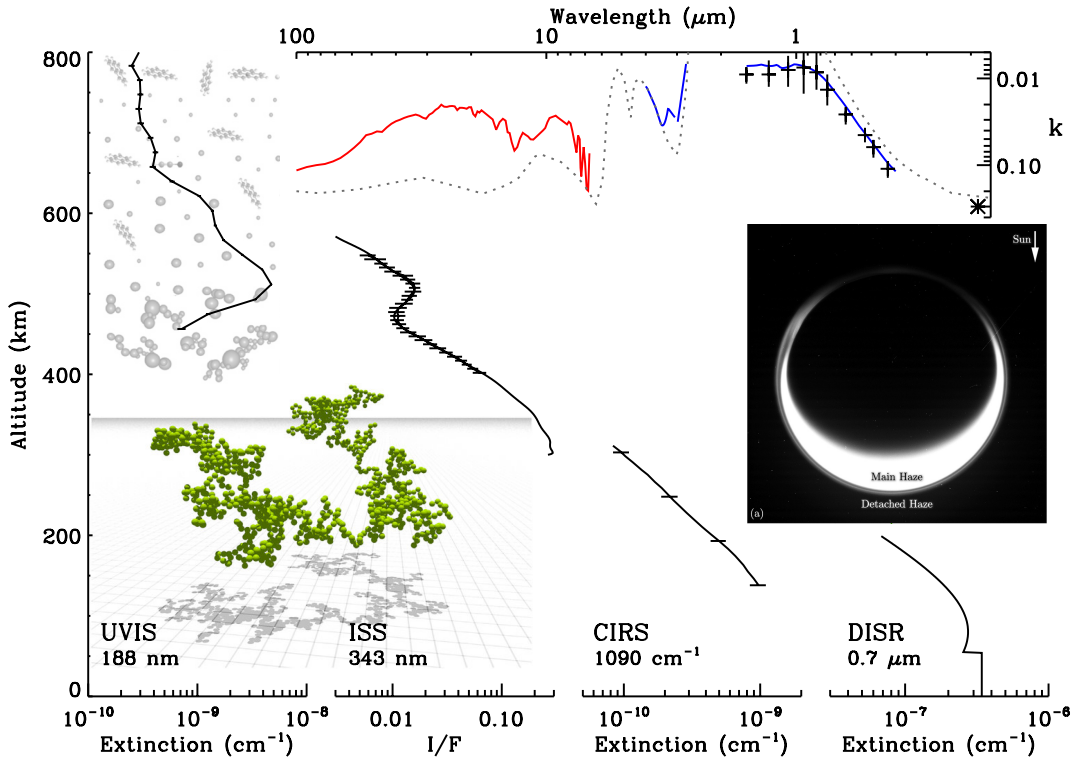

Figure 7: Haze observations from Cassini-Huygens instruments sensitive to different altitudes in Titan's atmosphere, including haze extinction profiles from UVIS (Koskinen et al., 2011) and CIRS (Vinatier et al., 2010a) observations, haze scattering from ISS observations (Seignovert et al., 2017) and haze optical depth derived from the in-situ DISR observations (Doose et al., 2016). The inset Titan image from ISS observations highlights the main and detached haze layers (Seignovert et al., 2017). The background in the UVIS observations indicates the haze formation in the upper atmosphere and the gradual transition from spheres to aggregates near the detached haze layer according to theoretical simulations (Lavvas et al., 2011c). In the main haze layer particles are aggregates with $D_f \sim 2$ similar to the one presented in the lower left (Tazaki, 2021). The upper right panel presents the retrieved imaginary refractive index of Titan's haze (red: Vinatier et al. (2012), blue: Rannou et al. (2010), black: Lavvas et al. (2010)), compared to a typical tholin spectrum (dotted line: Khare et al. (1984)).

nitrogen containing PAHs (PANHs) are also detected as constituents of tholins (e.g. Mahjoub et al., 2016; Maillard et al., 2020; Schulz et al., 2021, and references therein).

The large mass positive and negative ions are abundant enough to affect the atmospheric electron balance below the ionospheric peak, as demonstrated by the combination of INMS, CAPS, RPWS/LP observations (Robertson et al., 2009; Wahlund et al., 2009). At the deepest flybys, observations suggest that the ionosphere behaves like a dusty plasma where the free electrons are attached to the large molecules and the electron balance is defined by the equilibrium between the positive and the large negative ions (Michael et al., 2011; Ågren et al., 2012; Lavvas et al., 2013; Vigren et al., 2014; Shebanits et al., 2016; Chatain et al., 2021a,b). The shift in the type of the charge balance has important ramifications for the subsequent haze growth. On the one hand recombination is driven by collisions between two types of ion populations, which is a significantly slower process than the corresponding recombination with free electrons, therefore allowing for a longer lifetime of the charged ions. On the other hand, the ion recombination can induce a partial mass transfer from the small mass positive ions to the charged macromolecules that allows for the rapid mass growth of the latter. As the large molecules continue to grow, their interaction with the radiation field (through photoionization and photodetachement) and the charge populations (electrons and ions) results in a charge distribution that contains positive, neutral, and negative values. Numerical simulations of these processes (Lavvas et al., 2013) demonstrate that they can reproduce both the negative and positive macromolecule populations observed by the Cassini instruments at multiple altitudes in Titan's ionosphere (Fig. 4). Nevertheless, the estimated mass flux from the heavy ions is ∼10% of the haze mass flux observed in the lower atmosphere (Wahlund et al., 2009). Therefore these rapidly formed, large molecular structures are the pivot point beyond which further chemical growth and coagulation lead to haze particle growth at the sizes observed in the deeper atmosphere.

5.1.2 Surface growth

Right below the in situ probed ionosphere, remote-sensing haze characterisation is difficult as the particles are too small to significantly affect the electromagnetic field. Only at short wavelengths (UV) the particle opacity is comparable to the atmospheric opacity (particularly between 180 and 190 nm), and information for the haze properties could be derived through stellar and solar occultations with the UVIS instrument (Liang et al., 2007; Koskinen et al., 2011; Capalbo et al., 2016; Fan et al., 2019). UV occultations are sensitive to the combined effect of particle size, particle number density, and particle refractive index as these parameters define the particle opacity, and their analysis demonstrates the increase of the particle opacity from the lower thermosphere (∼700 km) to the mid-mesosphere (∼400 km). Towards the lower end of the altitude range haze particles are large enough to be probed with other Cassini instruments, particularly through the UV (∼300 nm) and visible (∼600 nm) filters of the ISS broadband imaging. These observations complement the UV occultations and expand our understanding of haze distribution through a broad spatial and temporal characterisation that revealed the variability of the haze properties. The most striking variability is observed in a detached haze layer that over the course of the Cassini mission dropped from a location near 500 km altitude (Porco et al., 2005) at the beginning of Titan's exploration by Cassini in 2004, to suddenly at 300 km in 2009 (West et al., 2011), and even disappeared in 2012 before reappearing in 2016 (West et al., 2018). In the detached layer, particles are expected

to be composed of small spherical particles and of small aggregates of such primary particles and have a mass flux equivalent to that observed in the main haze layer (Lavvas et al., 2009; Cours et al., 2011; Seignovert et al., 2017). Thus, the particles mass growth due to transition from the gas to the solid phase is approximately completed at this location, i.e. below ∼500 km.

As the ion populations are rapidly reduced below the ionosphere, the haze growth should proceed through neutral processes on the surface of the formed embryos. However, the nature of these heterogeneous interactions is not well understood, although some experimental results are now becoming available (Hong et al., 2018). A large population of radicals is produced by the photo-dissociation of multiple species in Titan's upper atmosphere (Vuitton et al., 2019). The high chemical potential of these radicals in combination with the long residence time of the haze embryos (∼10 days), due to Titan's low gravity field and the particle small size (∼nm), can outbalance the lower rates of neutral relative to ion reaction rates and allow for an efficient increase of the haze mass flux below the ionosphere. Theoretical studies of such processes based on the growth of polycyclic aromatic compounds through radical reactions suggest that this mechanism could be efficient in Titan's upper atmosphere (Lavvas et al., 2011c). However, the formation processes for large aromatic molecules are uncertain and this highlights the need for new inputs from laboratory studies to reach an understanding of the chemistry occurring in Titan's atmosphere. Moreover, closed-shell molecules could also heterogeneously interact on the surface of the haze embryos, if the latter are activated (also known as particle ageing) during their interaction with the high-energy photons reaching Titan's upper atmosphere (Dimitrov and Bar-Nun, 2002; Courtin et al., 2015), but this mechanism has not been investigated in detail. Laboratory studies based on tholins have provided some preliminary indications for the impact of high-energy radiation on the evolution of the optical properties and on the photoionization of the particles (Carrasco et al., 2018; Tigrine et al., 2018), but further studies are required for understanding their global impact on haze formation. Another important consequence of the heterogeneous processes on the particle surface has to do with their shape. Haze particles stick to each other when they collide allowing the formation of aggregates. However, the mass added to such aggregates during their heterogeneous interaction with the gas phase can return the particles to a quasi-spherical shape (Morgan et al., 2007). Simulations of such interactions for Titan's haze demonstrate that above 500 km the combination of the small particle size with the large inventory of radical species formed by the photochemistry results in a quasi spherical growth of the haze particles reaching a radius of ∼50 nm (Lavvas et al., 2011c). In conclusion, we see that both ion and neutral chemistry contributions are important for the formation and growth of Titan's haze, the first for initiating the haze formation, and the second for defining the final mass flux and the shape and the size of the formed haze particles.

5.1.3 Coagulation

Below 500 km altitude coagulation further increases the size of the particles at the expense of their number density, which causes their shape to obtain an aggregate structure of quasi-spherical primary particles. At these larger particle sizes, the haze characterisation is also possible at longer wavelengths from visible to thermal IR. Light scattering and polarization measurements at visible and near IR wavelengths inside Titan's atmosphere with Huygens/DISR verified that the haze particles in the deep atmosphere (below 150 km) are aggregates that can

be described by a fractal distribution of 40–50 nm radius primary particles (Tomasko et al., 2008; Tomasko and West, 2009; Doose et al., 2016). The particle shape can be mathematically described through a fractal dimension, D_f, that relates to the way the primary particles are distributed within the aggregate, and takes values between 1 (for linear aggregates) and 3 (for compact spherical aggregates). The analysis of the in situ observations suggested that the aggregates are composed of a few thousand primary particles with a distribution that is consistent with a D_f=2. However, more recent studies suggest that the particle fractal dimension may be slightly higher, D_f=2.3–2.4 (Coutelier et al., 2021). Assuming the dominance of aggregation below 500 km, pure haze microphysics models (Lavvas et al., 2010; Rannou et al., 2010) can reproduce the observed haze optical properties across the various wavelengths observed with the Cassini instruments. These simulations describe the coagulation of the particles as a process dominated by their random collisions (Brownian coagulation). Moreover, due to their interaction with the radiation field as well as the ion and electron populations formed in the deep atmosphere from the deposition of cosmic rays (Molina-Cuberos et al., 1999), haze particles can accumulate a charge on their surface that results in their mutual repulsion, thus affecting and eventually limiting their growth. The microphysical models require a haze mass flux of 3×10^{-14} g cm^{-2} s^{-1} (referred to the surface) and a charge to radius ratio of 15 e$^-$/μm to reproduce the observed haze opacity spectrum and scattering properties. The particle charging eventually results in a constant particle size in the deep atmosphere with an effective radius of 2–3 μm.

5.1.4 Composition

The analysis of the DISR observations (Lavvas et al., 2010; Rannou et al., 2010) revealed that optical properties of Titan's haze material are similar, although not completely identical, to the laboratory produced haze analogs (e.g. Khare et al., 1984, see Fig. 7 inset). Their optical properties in the visible and near ultraviolet are controlled by $\pi - \pi^*$ and $n - \pi^*$ electronic transitions, resulting in a broad absorption continuum that gives the analogues an orange-brown color (Imanaka et al., 2004; Gavilan et al., 2018). Similar differences in the optical properties were also found in the analysis of VIMS and CIRS observations that expanded the haze characterisation towards the thermal IR. These observations indicated that Titan's haze has a lower absorptivity at thermal wavelengths compared to the laboratory analogs, while the spectral features observed imply the dominance of C-C and C-H bonds seconded to a lesser degree by C-N bonds. On the contrary, the pyrolysis experiment of Huygens/GCMS at 600 K revealed a product composition dominated by NH_3 and HCN, suggesting that N is abundantly incorporated in the refractory core of the haze structure (Israël et al., 2005). A reconciliation of these contradictory results may come from the ageing of the particles during their fall in Titan's atmosphere through their interaction with high energy photons, hydrogen and ions as suggested by laboratory experiments (Carrasco et al., 2018; Chatain et al., 2020). Such ageing processes are also suggested by the variation of aromatic and aliphatic signatures in the VIMS spectra between 3.3 and 3.4 μm (Courtin et al., 2015). However, Biemann (2006) set in question the Israël et al. (2005) conclusion from the GCMS observations regarding the strong nitrogen incorporation in the haze.

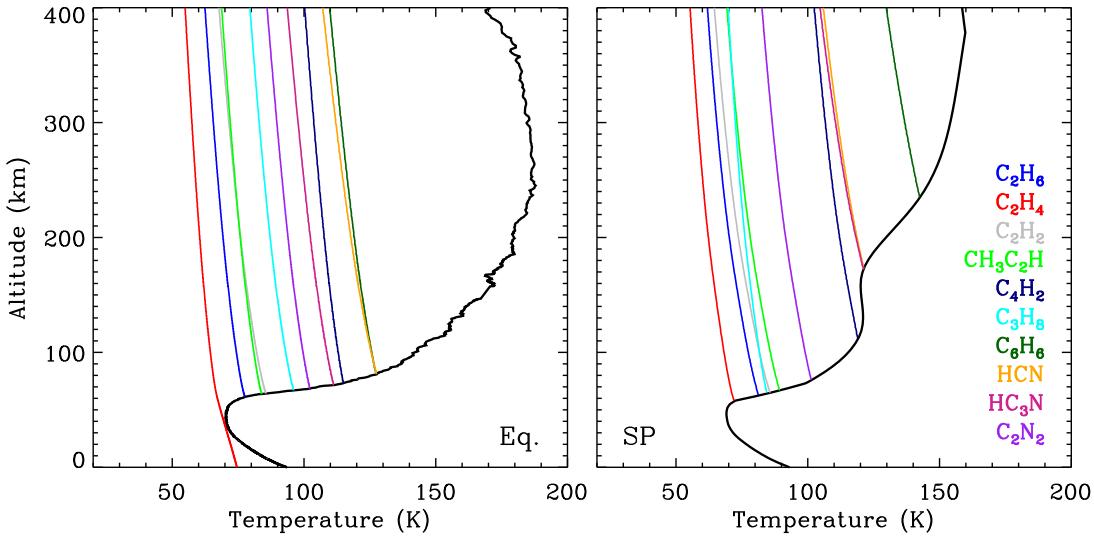

Figure 8: Condensation curves at equatorial (Huygens landing site, Fulchignoni et al., 2005) and winter south pole (80°S, September 2014, Teanby et al., 2019) conditions in Titan's atmosphere. The intercept of each colour line with the local temperature profile (solid black lines) shows the approximate location of condensation of each photochemical product. The higher local gas abundances and associated lower temperature over the south pole allows for condensation at higher altitudes, relative to the equatorial conditions.

5.1.5 Feedback mechanisms

The nature of the haze formation process makes evident the strong interaction of the haze with the gas phase chemistry. The observed haze mass flux corresponds to ∼30% of the mass flux generated from the photolysis of methane and nitrogen (Lavvas et al., 2011a), therefore the haze formation is a significant component of the atmospheric photochemistry. But there are additional feedback mechanisms: as the haze is optically thick in the lower atmosphere it modifies the gas species photolysis rates, while it may also affect their abundance through the heterogeneous reactions on its surface (Vuitton et al., 2019). Furthermore, haze particles interact strongly with the radiation field, therefore affect the thermal structure of the atmosphere and the radiation reaching the surface, as well as the global circulation patterns. This is well established for Titan's lower atmosphere where the haze particles partake in heating the stratosphere and cooling the surface (West et al., 2014), as well as defining the global energy balance (García Muñoz et al., 2017). However, the role of the nascent haze particles in the thermal structure of the upper atmosphere is still under investigation. At those altitudes haze particles have smaller sizes, but higher populations than in the lower atmosphere, while their optical properties are unknown. Further analyses of Cassini observations and laboratory studies are required to decipher the optical properties of the particles and their role in the energy balance of Titan's upper atmosphere.

5.2 Stratospheric Ice Clouds

At the decreasing temperatures of the lower stratosphere and troposphere, the sedimenting haze particles act as nucleation sites for the condensation of the produced photochemical gases. CIRS observations clearly demonstrate this process with the signature of organic condensates near 160 cm^{-1} (attributed to HCN and HC_3N) and 80 cm^{-1} (attributed to C_2H_6) detected at the altitudes were their condensation is anticipated based on the observed gas abundances and atmospheric temperature (Anderson and Samuelson, 2011; de Kok et al., 2010). The abundance of the condensates increases towards the winter pole although their presence is detected at various latitudes (Fig. 8). VIMS spectral images reveal a broad C_2H_6 cloud over the north (winter) pole in 2005 (Griffith et al., 2006), as well as an HCN cloud in 2012 over the south (winter) pole (de Kok et al., 2014); in 2011 CIRS observations reveal a C_6H_6 cloud at the south pole (Vinatier et al., 2018), while other cloud features were sporadically detected at lower latitudes (Griffith et al., 2005; Rodriguez et al., 2009). At northern winter latitudes, a broad aerosol feature centered on 220 cm^{-1} becomes prominent and is likely due to condensation of nitrile species (de Kok et al., 2007b, 2008; Anderson and Samuelson, 2011; Anderson et al., 2018). At the Huygens landing site at Titan's equator, the retrieved particle properties reveal a clear change in the spectral behaviour of the particles below 80 km suggesting the contribution of different condensing gases (Tomasko et al., 2008; Doose et al., 2016). Experiments with Titan tholins demonstrate that the nucleation efficiency of the haze analogs is high (Curtis et al., 2008; Rannou et al., 2019; Yu et al., 2020). Theoretical studies for cloud formation at the equatorial conditions of the Huygens landing site suggest that the variation of the haze wavelength opacity below 80 km could be correlated with the condensation of the most abundant photochemical products HCN and C_2H_6, while below 30 km the co-condensation of N_2-CH_4 dominates the condensate opacity (Barth, 2006; Lavvas et al., 2011b). At higher latitudes, condensates of C_6H_6 and nitriles can form at higher altitudes depending on the local temperature conditions and gas abundances driven by the seasonal changes (Dubois et al., 2021; Nna-Mvondo et al., 2019; Nna-Mvondo and Anderson, 2022; Vinatier et al., 2018). A C_6H_6/C_2H_2/HCN co-crystal has also been predicted theoretically (Ennis et al., 2020).

In laboratory studies simulating the conditions of Titan's stratosphere, solid ices have been exposed to long-UV photons ($\lambda > 120$ nm) and their evolution has been characterized by infrared spectroscopy and mass spectrometry. Photo-processing of pure benzene ice generates more than a dozen aliphatic and aromatic hydrocarbons (Mouzay et al., 2021b). Simulations of the photochemical aging process undergone by ices demonstrate the possibility of a solid-state formation pathway of nitrile derivatives from the photo-processing of C_6H_6:HCN ices (Mouzay et al., 2021a). The photochemistry of ethyl cyanide (CH_3CH_2CN) ices has also been investigated. Several photoproducts, such a simple hydrocarbons, nitriles and methylketenimine have been identified in the solid phase (Couturier-Tamburelli et al., 2018b). It has been found that HCN and C_2H_2 ices are photochemically inert alone, but react when accreted on Titan's aerosol analogs, resulting in incorporation of acetylene or HCN into the aerosol analogues (Couturier-Tamburelli et al., 2018a; Fleury et al., 2019). This important molecular diversity can either be transported as ices toward the surface or be released in the gas phase. For a detailed review of the post-Cassini knowledge regarding ice clouds, with perspectives from both observational and experimental standpoints, see Anderson et al. (2018).

6 Middle Atmosphere Dynamics

6.1 Zonal Winds

Titan is tidally locked, so has a length of day tied to its orbital period of 15.9 days around Saturn. This slow rotation places Titan's atmosphere in the cyclostrophic regime, where pressure gradients are balanced by the centrifugal force, rather than the more conventional geostrophic balance where pressure gradients are balanced by the Coriolis force. Titan and Venus thus share some similarities in their global dynamics, with super-rotating winds first inferred from stellar occultations (Hubbard et al., 1993). Titan's equatorial wind profile was measured in-situ using the Huygens probe Doppler Wind Experiment at ∼10°S, confirming the super-rotation of Titan's stratosphere and measuring zonal wind speeds of up to 100 m s^{-1} in the lower stratosphere (Bird et al., 2005). GCMs can reproduce this super-rotation and also predict a zonal symmetry in Titan's atmosphere (Hourdin et al., 1995; Newman et al., 2011; Lebonnois et al., 2012; Lombardo and Lora, 2022).

The Huygens wind measurements also revealed a lower stratosphere zonal wind minimum at ∼75 km/20 mbar (Bird et al., 2005). Some GCMs are able to reproduce this wind minimum, although the magnitude of the reduction is much less than observed by Huygens (Lebonnois et al., 2012). It is also impossible to know with one descent profile whether the lower stratosphere wind minimum is a global feature. Interestingly, this pressure level is approximately where radiative time scales transition from greater than to less than one Titan year, so it could represent the boundary between distinct dynamical regimes (Lebonnois et al., 2012).

More detailed spatial and seasonal coverage was possible with Cassini's remote sensing instruments. In particular Cassini/CIRS mapping observations have been used extensively to determine the zonal behaviour of Titan's stratospheric temperature and composition (Teanby et al., 2006; Achterberg et al., 2008b; Achterberg et al., 2011; Sharkey et al., 2021). These observations show Titan's stratosphere to be largely zonally symmetric. However, the symmetry axis of Titan's stratosphere seems to be offset from axis of rotation by around 4° (Achterberg et al., 2008a; Teanby et al., 2010a; Sharkey et al., 2020). This feature is also visible in the aerosol distribution observed with ISS (Roman et al., 2009), which does not currently have a convincing explanation and is currently an open question (Nixon et al., 2018). The zonal symmetry means thermal wind balance equations can be used to infer wind velocities in the stratosphere and mesosphere (Flasar et al., 2005; Achterberg et al., 2008b; Teanby et al., 2008; Achterberg et al., 2011; Vinatier et al., 2020; Sharkey et al., 2021). This approximation breaks down close to the equator, but has been successfully used to determine zonal winds speeds of up to 200 m s^{-1} at mid-to-high latitudes. More recent work has used Doppler shifts in high spectral resolution ALMA observations to infer a very fast (∼340 m s^{-1}) zonal jet in the equatorial thermosphere (Lellouch et al., 2019; Cordiner et al., 2020). This jet appears to be unstable and repeated observations exhibit very large changes in velocity over short timescales, with the jet speed roughly halving over a period of 9 months ($\Delta L_s \sim 8°$) (Cordiner et al., 2020). This shows Titan's atmospheric dynamics can react quickly to changes in seasonal forcing, especially at high altitude.

6.2 Meridional Circulation

Meridional circulation is used to describe the large-scale circulation in Titan stratosphere and mesosphere in the latitudinal direction. Vertical motions in Titan's middle atmosphere are difficult to measure directly, with vertical velocities of order a few mm s^{-1} predicted by GCMs (Luz et al., 2003; Lombardo and Lora, 2022) near to the stratopause at ∼0.1 mbar. However, as an alternative, trace gas species can be used effectively as tracers of vertical motion. Most trace species in Titan's atmosphere have a vertical gradient due to their upper atmosphere photochemical source combined with a lower stratosphere condensation sink (Vuitton et al., 2019). Subsidence will advect these profiles downwards and result in enhanced abundances at lower altitudes. This enrichment can be detected by remote sensing, with the magnitude of enrichment being a measure of the vertical velocity (Teanby et al., 2012). Gases with shorter lifetimes tend to have steeper gradients and increased sensitivity to subsidence (Teanby et al., 2009, 2010b). This method was used to infer velocities of a few mm s^{-1} in the mesosphere over Titan's south pole in southern winter (Teanby et al., 2012; Vinatier et al., 2015; Teanby et al., 2017; Vinatier et al., 2020), which is broadly consistent with predictions from GCMs. Alternatively, adiabatic heating caused by compression of the air as it moves deeper in the atmosphere can also be observed with remote sensing and give an independent and comparable estimate of subsidence velocity over the poles (Achterberg et al., 2011; Teanby et al., 2012). At low latitudes (±30°N), energy balance considerations suggest velocities of similar magnitude. Upwelling velocities of -0.5 – 1.5 mm s^{-1} at ∼1 mbar are required to match radiative balance model predictions to the observed temperature profile, with the exact velocity depending on latitude and season (Bézard et al., 2018).

Methane has a long photochemical lifetime, so is expected to be well mixed in the stratosphere. However, careful scrutiny of the CIRS observations suggest that methane in Titan's lower stratosphere may not be entirely constant and could in fact vary in abundance with latitude from 1–1.5%. This is potentially linked to convective events in the lower atmosphere or secondary meridional circulation cells (Lellouch et al., 2014).

There have been many studies of the seasonal variation of trace gases species and temperature observed during Cassini's mission (e.g. Flasar et al., 2005; Coustenis et al., 2010; Teanby et al., 2010c; Vinatier et al., 2010b; Achterberg et al., 2011). The most recent and complete studies, using observations spanning the entire mission are: Sylvestre et al. (2018); Teanby et al. (2019); Coustenis et al. (2020); Mathé et al. (2020); Vinatier et al. (2020); Sharkey et al. (2021). Illustrative temperature, HCN, and HC_3N seasonal changes are shown in Figure 9. These observations are extremely valuable for determining how the meridional circulation changes with seasons. Evidence for subsidence-driven trace gas enrichment at the south pole almost immediately after the 2009 equinox indicated that Titan's stratosphere can react extremely quickly to changes in solar heating (Teanby et al., 2012). There was also evidence for two circulation cells developing about 6–12 months after the 2009 equinox (Vinatier et al., 2015), in agreement with GCM predictions. Between equinoxes the distribution of trace gases indicate middle atmosphere circulation comprises large hemisphere-to-hemisphere cells, with upwelling in the summer hemisphere and subsidence close to the winter pole (Teanby et al., 2019). However, there may be a small residual secondary cell close to the pole in spring, which can retain some of the enriched gases after the polar vortex has dissipated (Vinatier et al., 2020).

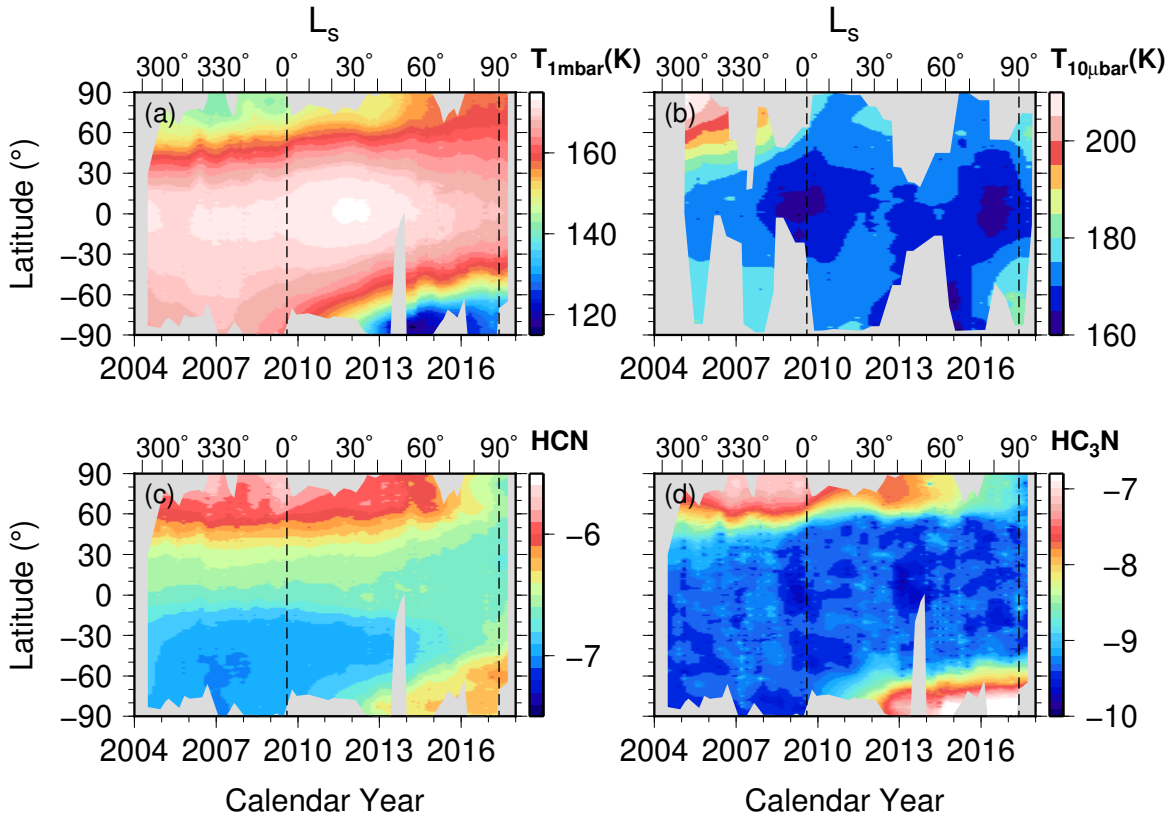

Figure 9: Seasonal changes in temperature and composition from Cassini/CIRS observations. (a) Temperature in the mid-stratosphere at 1 mbar from nadir observations (Teanby et al., 2019). At this pressure level Titan's winter poles are cold and exhibit strong seasonal variations, whereas the equator is relatively warm and more stable. (b) Temperature at 10 μbar near the stratopause from limb observations (Teanby et al., 2017). At this lower pressure adiabatic heating from subsidence over the poles causes warm winter poles, although this takes a while to develop in the south due to enhanced radiative cooling. (c,d) HCN and HC_3N $\log_{10}$ volume mixing ratio (VMR) at 1 mbar from nadir observations (Teanby et al., 2019). These gases act as tracers of vertical motion, with subsidence causing increased VMR. Short lifetime gases such as HC_3N are more sensitive to subsidence than longer lifetime gases such as HCN and exhibit more extreme enrichment. Grey areas show gaps in coverage and dashed vertical lines are the northern spring equinox ($L_s = 0°$) and northern summer solstice ($L_s = 90°$).

6.3 Polar Vortices

Polar vortices are prominent features of all planets with an atmosphere in our solar system (Mitchell et al., 2021). They are regions of very high middle-atmosphere prograde winds that encircle the pole, are driven by cooling-induced pressure gradients combined with conservation of angular momentum, and can act as effective mixing barriers that allow air masses with distinct composition to form. Typically vortices are most intense in the winter hemisphere as temperature differences are more extreme.

Just after Cassini entered the Saturn system in 2004, observations of trace gas enrichment and a hot stratopause at Titan's north pole showed a north polar winter vortex was well established (Flasar et al., 2005). Short lifetime species such as HC_3N and C_4H_2 had polar abundances enriched by orders of magnitude compared to the equator, and there appeared to be a direct correlation between species lifetime and enrichment factor (Teanby et al., 2009, 2010b). This is because the shorter the species lifetime the steeper the vertical profile and the more enrichment occurs during subsidence. The north polar stratopause region was also much hotter than at the equator due to subsidence-induced adiabatic heating (Flasar et al., 2005; Achterberg et al., 2008b; Teanby et al., 2008).

Further insight into vortex structure could be derived by using the measured temperature field and thermal wind balance to derive zonal wind speeds and potential vorticity (Flasar et al., 2010). Zonal wind speeds in the vortex jet were close to 200 m s^{-1} at $\sim$30°N (Achterberg et al., 2011). Furthermore, potential vorticity gradients were steepest at $\sim$60°N, indicating horizontal mixing is inhibited at this latitude (Teanby et al., 2008; Achterberg et al., 2011). This suggests Titan's polar air mass could have a distinct composition, with potentially exotic chemistry occurring poleward of this boundary. A clear boundary in trace gas composition is indeed present at $\sim$60°N in northern winter, showing the isolation of the polar air mass (for example HCN and HC_3N in Figure 9). However, Titan's vortex appears to also be quite leaky, with moderate lifetime gases such as HCN able to escape the vortex to lower latitudes (Teanby et al., 2008). There is also a suggestion of an annular structure to Titan's North polar vortex (Achterberg et al., 2011; Sharkey et al., 2021). This is not considered a stable configuration and requires some process to maintain, such as latent heat release by condensation, as is observed on Mars (Scott et al., 2020). Polar trace gas enrichment began to steadily decline after equinox, indicating a post-equinox weakening of the northern vortex. However, north polar enrichment of trace gases was visible up until summer solstice, much longer than expected, and suggesting that vortex enrichment is relatively long-lived (Teanby et al., 2019).

At the south pole, formation of the southern winter vortex began almost immediately after equinox. The first signs of vortex formation were high altitude enrichment of short lifetime gases such as HC_3N (Teanby et al., 2012; Vinatier et al., 2015). This enrichment coincided with subsidence-induced adiabatic heating in the mesosphere. The enrichment and heating over the south pole increased as the vortex developed. However, approximately two years after equinox there was an unexpected rapid cooling of the mid-stratosphere to mesosphere region, which was not predicted by GCMs and lasted for around four years (Teanby et al., 2017). This cooling led to the creation of south polar HCN and benzene ice clouds (de Kok et al., 2014; Vinatier et al., 2018). A possible explanation for this unexpected cooling is that extreme enrichment of trace gases developed in subsiding air during vortex formation can act as efficient infrared coolers, and the effect of this extra radiative cooling is enough to offset the

heating effect of adiabatic compression (Teanby et al., 2017). However, after a few years the vortex and meridional circulation becomes more fully developed, and the subsidence velocity becomes sufficient for adiabatic heating to again dominate over radiative cooling. By the end of the Cassini mission the southern vortex was developing a similar temperature structure to the northern winter vortex seen at the start of the mission, with a hot stratopause and trace gas enrichment (Teanby et al., 2017; Teanby et al., 2019; Vinatier et al., 2020). A schematic of the vortex evolution is shown in Figure 10.

6.4 Haze Spatial Distribution

Beyond the general picture of haze formation and growth in the vertical direction (see discussions in Section 5.1), there is horizontal variability in the haze distribution driven by the season evolution of Titan's atmosphere. General circulation models have captured the broad picture of atmospheric ascent from the summer hemisphere and descent on the winter hemisphere and how this global circulation affect the distribution of haze and cloud particles (Rannou et al., 2004, 2006; Rodriguez et al., 2009; Lebonnois et al., 2012; Larson et al., 2014; Larson, 2019). The most characteristic feature of this seasonal variability is the evolution of the detached haze layer during the Titan year. According to the circulation models, this distinct haze feature is formed by the equilibrium between the particle sedimentation and their transport by the horizontal circulation between the two poles (Rannou et al., 2002). During equinox, the reversal of the circulation results in a temporary diminishing of the horizontal transport, thus allowing for a free fall of the particles and eventually the disappearance of the detached layer, consistent with the Cassini observations (West et al., 2018). The models also broadly predict correctly the reappearance of the layer as observed in the observations, although the details of the observed vertical structure of the detached layer provide additional constraints that will be useful for future studies. Seasonal changes propagate to the main haze layer as well and cause a periodic North-South asymmetry in the atmospheric brightness due to changes in the haze opacity. Cassini CIRS and VIMS observations allowed for a broad spatial and temporal investigation of the stratospheric main haze layer, beyond the snapshot obtained at the Huygens landing site (Rannou et al., 2010; Vinatier et al., 2010a, 2012; Anderson and Samuelson, 2011). The results demonstrate that Titan's haze optical properties are similar at the various latitudes/altitudes investigated, suggesting a homogeneous chemical composition. Nevertheless, the haze opacity distribution presents horizontal variations that reflect the seasonal variations of the global circulation, as well as, the local conditions occurring at the polar vortices (Vinatier et al., 2015, 2020). Combining observations from Cassini and the Hubble Space Telescope covering half a Titan year, Karkoschka (2022) demonstrated that the observed asymmetry is clearly related to Titan's seasons, with different periods for haze at altitudes above 150 km and below 80 km.

7 Conclusions: the Future of Titan's Atmosphere Exploration

Post Cassini-Huygens, we are now able to look back on the scientific questions from the beginning of the mission, and assess the progress that has been made towards answering them. Cassini-Huygens fully revealed Titan's remarkable nature and successfully achieved the primary mission objectives, including:

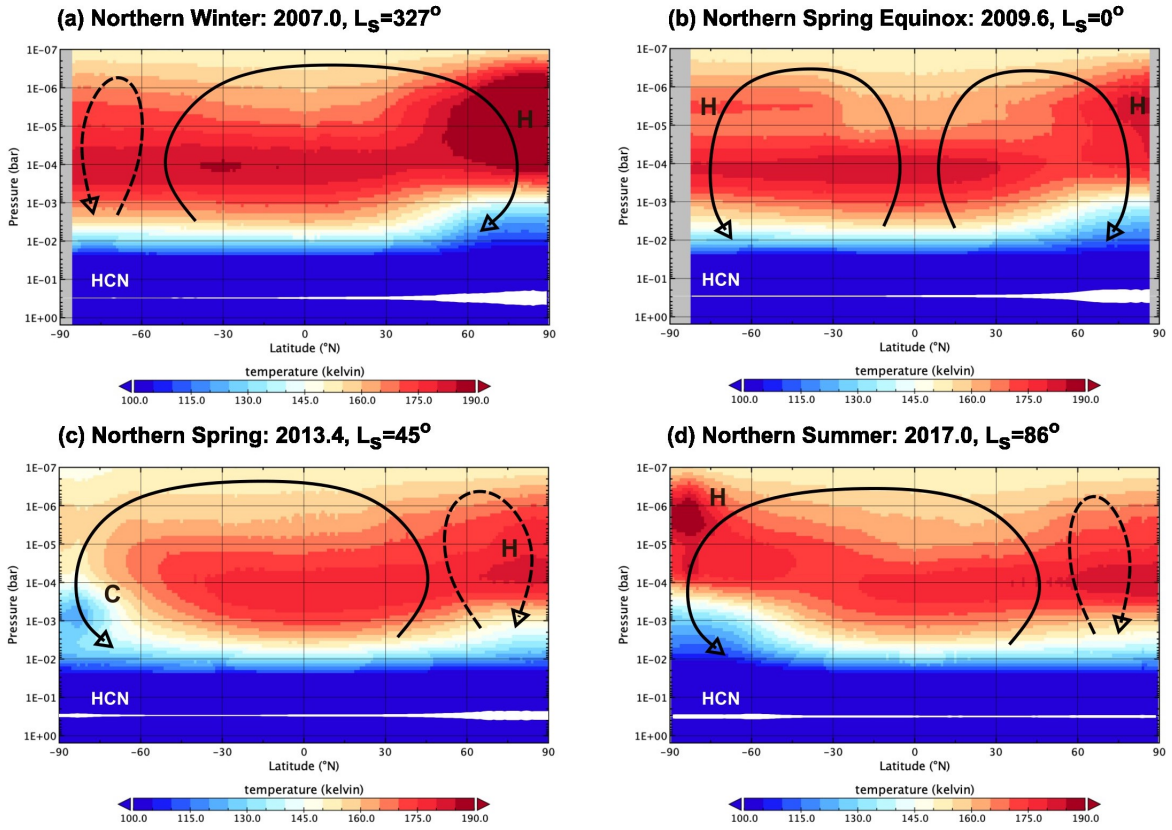

Figure 10: Schematic of Titan's middle-atmosphere circulation. Colours show temperature measurements from Cassini/CIRS (Teanby et al., 2019). White lines thickness is proportional to HCN abundance at 1 mbar and gives an idea of trace gas enrichment. "H" indicates subsidence-induced adiabatic heating, "C" indicates enhanced radiative cooling from polar trace gas enrichment, and arrows indicate inferred approximate circulation direction. For most of Titan's year the circulation is dominated by a single large hemisphere-to-hemisphere circulation cell, potentially with a small secondary circulation cell near the summer pole. The southern hemisphere cold polar mesopause region in north spring (southern fall), labelled "C", was unexpected and suggests enhanced cooling from trace gases dominates over heating from subsidence until the winter vortex is well established. Underlying data from Cassini/CIRS netCDF database (Teanby et al., 2019) and plotted using NASA's Panoply software (`https://www.giss.nasa.gov/tools/panoply`).

- determine the abundance of the atmospheric constituents, including noble gases and isotope ratios;
- measure the vertical and horizontal distribution of trace gases, discover complex organic molecules, characterize aerosol layers and determine their properties, investigate ice cloud composition;
- measure the winds and global temperatures, observe formation and break-up of the winter polar vortex;

The Cassini mission extensions allowed the monitoring of seasonal changes, in particular the complete reversal of global atmospheric dynamics as Titan moved from southern summer to northern summer solstice. Following the changing solar illumination, Cassini revealed important variations in trace gases, aerosols, clouds, temperature and winds.

This first detailed look at Titan's atmosphere raised many important scientific questions for future investigations:

- What is the vertical and latitudinal variation in methane's abundance in the lower stratosphere, how does it vary with season, and how is the methane humidity influenced by dynamical redistribution?
- What generates the atmospheric super-rotation and what maintains it? Why is the atmospheric rotation axis tilted?
- How do the polar vortices form, evolve, and dissipate? Can enhanced radiative cooling fully explain the extremely cold stratospheric and mesospheric temperatures observed during vortex formation?
- Does all the oxygen in Titan's atmosphere originate from Enceladus or are there other sources?
- What are the most complex molecules attained by the chemistry? Are they mostly hetero-polyaromatic compounds? Are there any of prebiotic relevance? What is the impact of heterogeneous chemistry on the stratospheric gas composition?
- What are the composition (amount of nitrogen and oxygen incorporation), optical properties and spatial distribution of the haze? What is the composition (pure or mixed condensates) of the stratospheric ice clouds and what is their seasonal variability?

To fully answer these questions will require a dedicated Titan orbiter and in-situ exploration (e.g. Coustenis et al., 2009; Tobie et al., 2014; Mitri et al., 2018; Rodriguez et al., 2022). In the medium term the Dragonfly mission will provide valuable in-situ exploration of the surface and lower atmosphere (Barnes et al., 2021). The eventual fate of stratospheric organics is the lower atmosphere and surface, so in-situ mass spectrometry from the Dragonfly Mass Spectrometer (DraMS) will be particularly important for understanding atmospheric chemistry.

However, in the near term further astronomical measurements with ground and space-based telescopes can help to fill in gaps in our knowledge of Titan's atmospheric composition left by Cassini-Huygens. Important tools for investigation in the 2020s and 2030s include

the ALMA Observatory operating at millimater and sub-millimeter wavelengths, which has already proved adept at the detection of new molecules in the middle and upper atmosphere (Cordiner et al., 2015; Palmer et al., 2017; Nixon et al., 2020; Thelen et al., 2020). In the mid-infrared, the TEXES instrument (Texas Echelon Cross Echelle Spectrometer, Lacy et al., 2002) on NASA's Infrared Telescope Facility (IRTF) has recently yielded a first detection of propadiene (Lombardo et al., 2019b) and will be important for searching for symmetric molecules that have no dipole and are invisible in the sub-millimeter/rotational spectrum. The recently-launched James Webb Space Telescope (JWST) will also fill some gaps in spectroscopy left by Cassini's VIMS and CIRS instruments, particularly around 5.2–6.5 μm which is mostly opaque from the ground due to the Earth's atmosphere, as well as monitoring seasonal changes (Nixon et al., 2016). Such capabilities and those on the next generation of very large aperture telescopes on Earth will provide an important complement at infrared wavelengths to ALMA and other long wavelength interferometers (e.g. ngVLA). Together these facilities will be able to fully monitor seasonal changes in Titan middle atmosphere from Earth and provide the data needed to more fully understand the complex interplay between its chemistry and dynamics, its atmospheric evolution, and possibilities for astrobiology.

Acknowledgements

The authors thank B. Bézard, T. Koskinen and A. Solomonidou for their comments that improved the quality of the text and the figures.

References

Achterberg, R. K., Conrath, B. J., Gierasch, P. J., Flasar, F. M., Nixon, C. A., 2008a. Observation of a tilt of Titan's middle-atmospheric superrotation. Icarus 197, 549–555.

Achterberg, R. K., Conrath, B. J., Gierasch, P. J., Flasar, F. M., Nixon, C. A., 2008b. Titan's middle-atmospheric temperatures and dynamics observed by the Cassini Composite Infrared Spectrometer. Icarus 194, 263–277.

Achterberg, R. K., Gierasch, P. J., Conrath, B. J., Flasar, F. M., Nixon, C. A., 2011. Temporal variations of Titan's middle-atmospheric temperatures from 2004 to 2009 observed by Cassini/CIRS. Icarus 211, 686–698.

Ågren, K., Edberg, N. J. T., Wahlund, J.-E., May 2012. Detection of negative ions in the deep ionosphere of Titan during the Cassini T70 flyby. Geophysical Research Letters 39 (1), L10201.

Ågren, K., Wahlund, J. E., Garnier, P., Modolo, R., Cui, J., Galand, M., Müller-Wodarg, I., Dec. 2009. On the ionospheric structure of Titan. 57 (14-15), 1821–1827.

Anders, E., Grevesse, N., Jan. 1989. Abundances of the elements: Meteoritic and solar. 53 (1), 197–214.

Anderson, C., Samuelson, R., 2011. Titan's aerosol and stratospheric ice opacities between 18 and 500 m: Vertical and spectral characteristics from Cassini CIRS. Icarus 212, 762–778.

Anderson, C. M., Samuelson, R. E., Nna-Mvondo, D., 2018. Organic Ices in Titan's Stratosphere. Space Sci. Rev. 214 (8), 125.

Atreya, S.-K., Donahue, T.-M., Kuhn, W.-R., Aug. 1978. Evolution of a nitrogen atmosphere on Titan. Science 201, 611–613.

Barnes, J. W., Turtle, E. P., Trainer, M. G., Lorenz, R. D., MacKenzie, S. M., Brinckerhoff, W. B., Cable, M. L., Ernst, C. M., Freissinet, C., Hand, K. P., Hayes, A. G., Hörst, S. M., Johnson, J. R., Karkoschka, E., Lawrence, D. J., Le Gall, A., Lora, J. M., McKay, C. P., Miller, R. S., Murchie, S. L., Neish, C. D., Newman, C. E., Núñez, J., Panning, M. P., Parsons, A. M., Peplowski, P. N., Quick, L. C., Radebaugh, J., Rafkin, S. C. R., Shiraishi, H., Soderblom, J. M., Sotzen, K. S., Stickle, A. M., Stofan, E. R., Szopa, C., Tokano, T., Wagner, T., Wilson, C., Yingst, R. A., Zacny, K., Stähler, S. C., 2021. Science Goals and Objectives for the Dragonfly Titan Rotorcraft Relocatable Lander. Plan. Sci. J. 2 (4), 130.

Barth, E. L., Apr. 2006. Methane, ethane, and mixed clouds in Titan's atmosphere: Properties derived from microphysical modeling. Icarus 182 (1), 230–250.

Bell, J., Bougher, S., Waite Jr., J., Ridley, A., Magee, B., Mandt, K., Westlake, J., DeJong, A., Bar-Nun, A., Jacovi, R., Toth, G., De La Haye, V., Gell, D., Fletcher, G., 2011. Simulating the one-dimensional structure of Titan's upper atmosphere: 3. Mechanisms determining methane escape. J. Geophys. Res. 116, E11002.

Bellucci, A., Sicardy, B., Drossart, P., Rannou, P., Nicholson, P., Hedman, M., Baines, K., Burrati, B., 2009. Titan solar occultation observed by Cassini/VIMS: Gas absorption and constraints on aerosol composition. Icarus 201, 198–216.

Berry, J. L., Ugelow, M. S., Tolbert, M. A., Browne, E. C., Feb. 2019. Chemical Composition of Gas-Phase Positive Ions during Laboratory Simulations of Titan's Haze Formation. ACS Earth and Space Chemistry 3 (2), 202–211.

Bézard, B., 2014. The methane mole fraction in Titan's stratosphere from DISR measurements during the Huygens probe's descent. Icarus 242, 64–73.

Bézard, B., Nixon, C. A., Kleiner, I., Jennings, D. E., Nov. 2007. Detection of ^{13}CH $_3$D on Titan. Icarus 191 (1), 397–400.

Bézard, B., Vinatier, S., 2020. On the H_2 abundance and ortho-to-para ratio in titan's troposphere. Icarus 344, 113261.

Bézard, B., Vinatier, S., Achterberg, R. K., 2018. Seasonal radiative modeling of Titan's stratospheric temperatures at low latitudes . Icarus 302, 437–450.

Biemann, K., 2006. Complex organic matter in Titan's aerosols? Nature 444, E6.

Bird, M. K., Allison, M., Asmar, S. W., Atkinson, D. H., Avruch, I. M., Dutta-Roy, R., Dzierma, Y., Edenhofer, P., Folkner, W. M., Gurvits, L. I., Johnston, D. V., Plettemeier, D., Pogrebenko, S. V., Preston, R. A., Tyler, G. L., 2005. The vertical profile of winds on Titan. Nature 438, 800–802.

Bockelée-Morvan, D., Calmonte, U., Charnley, S., Duprat, J., Engrand, C., Gicquel, A., Hässig, M., Jehin, E., Kawakita, H., Marty, B., Milam, S., Morse, A., Rousselot, P., Sheridan, S., Wirström, E., Dec. 2015. Cometary Isotopic Measurements. 197 (1-4), 47–83.

Borucki, W., Whitten, R., 2008. Influence of high abundances of aerosols on the electrical conductivity of the Titan atmosphere. Planet. Space Sci. 56, 19–26.

Bourgalais, J., Carrasco, N., Vettier, L., Comby, A., Descamps, D., Petit, S., Blanchet, V., Gaudin, J., Mairesse, Y., Marty, B., Apr. 2021. Aromatic Formation Promoted by Ion-Driven Radical Pathways in EUV Photochemical Experiments Simulating Titan's Atmospheric Chemistry. Journal of Physical Chemistry A 125 (15), 3159–3168.

Bourgalais, J., Carrasco, N., Vettier, L., Pernot, P., Nov. 2019. Low-Pressure EUV Photochemical Experiments: Insight on the Ion Chemistry Occurring in Titan's Atmosphere. Journal of Geophysical Research (Space Physics) 124 (11), 9214–9228.

Broadfoot, A.-L., Sandel, B.-R., Shemansky, D.-E., Holberg, J.-B., Smith, G.-R., Strobel, D.-F., McConnell, J.-C., Kumar, S., Hunten, D.-M., Atreya, S.-K., Donahue, T.-M., Moos, H.-W., Bertaux, J.-L., Blamont, J.-E., Pomphrey, R.-B., Linick, S., Apr. 1981. Extreme ultraviolet observations from Voyager 1 encounter with Saturn. Science 212, 206–211.

Cable, M., Hörst, S., Hodyss, R., Beauchamp, P., Smith, M., Willis, P., 2012. Titan tholins: Simulating Titan organic chemistry in the Cassini-Huygens era. Chem. Rev. 112, 1882–1909.

Capalbo, F., Bénilan, Y., Fray, N., Schwell, M., Champion, N., Es-sebbar, E., Koskinen, T., Lehocki, I., Yelle, R., 2016. New benzene absorption cross sections in the VUV, relevance for Titan's upper atmosphere. Icarus 265, 95–109.

Carrasco, N., Tigrine, S., Gavilan, L., Nahon, L., Gudipati, M. S., Mar. 2018. The evolution of Titan's high-altitude aerosols under ultraviolet irradiation. Nature Astronomy, 1–6.

Chatain, A., Carrasco, N., Ruscassier, N., Gautier, T., Vettier, L., Guaitella, O., Jul. 2020. Interaction dust - plasma in Titan's ionosphere: An experimental simulation of aerosols erosion. 345, 113741.

Chatain, A., Wahlund, J. E., Shebanits, O., Hadid, L. Z., Morooka, M., Edberg, N. J. T., Guaitella, O., Carrasco, N., Aug. 2021a. Re-Analysis of the Cassini RPWS/LP Data in Titan's Ionosphere: 1. Detection of Several Electron Populations. Journal of Geophysical Research (Space Physics) 126 (8), e28412.

Chatain, A., Wahlund, J. E., Shebanits, O., Hadid, L. Z., Morooka, M., Edberg, N. J. T., Guaitella, O., Carrasco, N., Aug. 2021b. Re-Analysis of the Cassini RPWS/LP Data in Titan's Ionosphere: 2. Statistics on 57 Flybys. Journal of Geophysical Research (Space Physics) 126 (8), e28413.

Coates, A., Crary, F., Lewis, G., Young, D., Waite, J., Sittler Jr., E., 2007. Discovery of heavy negative ions in Titan's ionosphere. Geophys. Res. Lett. 34, L22103.

Coates, A., Jones, G., Lewis, G., Wellbrock, A., Young, D., Crary, F., Johnson, R., Cassidy, T., Hill, T., 2010. Negative ions in the Enceladus plume. Icarus 206, 618–622.

Coates, A., Wellbrock, A., Lewis, G., Jones, G., Young, D., Crary, F., Waite, J., 2009. Heavy negative ions in Titan's ionosphere: altitude and latitude dependence. Planet. Space Sci. 57, 1866–1871.

Cordiner, M., Nixon, C., Charnley, S., Mumma, M., Serigano, J., Palmer, M., Irwin, P., Teanby, N., Kisiel, Z., 2015. ALMA spectroscopy of Titan's atmosphere: First detections of vinyl cyanide and acetonitrile isotopologues. Bull. Am. Astron. Soc. 46, 205.03.

Cordiner, M. A., Garcia-Berrios, E., Cosentino, R. G., Teanby, N. A., Newman, C. E., Nixon, C. A., Thelen, A. E., Charnley, S. B., 2020. Detection of Dynamical Instability in Titan's Thermospheric Jet. Astrophys. J. Lett. 904 (1), L12.

Cordiner, M. A., Nixon, C. A., Charnley, S. B., Teanby, N. A., Molter, E. M., Kisiel, Z., Vuitton, V., May 2018. Interferometric Imaging of Titan's HC_3N, $H^{13}CCCN$, and $HCCC^{15}N$. The Astrophysical Journal Letters 859, L15 (6pp).

Cordiner, M. A., Nixon, C. A., Teanby, N. A., Irwin, P. G. J., Serigano, J., Charnley, S. B., Milam, S. N., Mumma, M. J., Lis, D. C., Villanueva, G., Paganini, L., Kuan, Y.-J., Remijan, A. J., 2014. ALMA Measurements of the HNC and HC_3N Distributions in Titan's Atmosphere. Astrophys. J. Lett. 795, L30.

Cottini, V., Nixon, C., Jennings, D., Anderson, C., Gorius, N., Bjoraker, G., Coustenis, A., Teanby, N., Achterberg, R., Bézard, B., de Kok, R., Lellouch, E., Irwin, P., Flasar, F., Bampasidis, G., 2012. Water vapor in Titan's stratosphere from Cassini CIRS far-infrared spectra. Icarus 220, 855–862.

Cours, T., Burgalat, J., Rannou, P., Rodriguez, S., Brahic, A., West, R. A., Nov. 2011. Dual Origin of Aerosols in Titan's Detached Haze Layer. The Astrophysical Journal Letters 741 (2), L32.

Courtin, R., Kim, S. J., Bar-Nun, A., Jan. 2015. Three-micron extinction of the Titan haze in the 250-700 km altitude range: Possible evidence of a particle-aging process. Astronomy and Astrophysics 573, A21.

Courtin, R., Sim, C., Kim, S., Gautier, D., 2012. The abundance of H2 in Titan's troposphere from the Cassini CIRS investigation. Planet. Space Sci. 69, 89–99.

Coustenis, A., Atreya, S. K., Balint, T., Brown, R. H., Dougherty, M. K., Ferri, F., Fulchignoni, M., Gautier, D., Gowen, R. A., Griffith, C. A., Gurvits, L. I., Jaumann, R., Langevin, Y., Leese, M. R., Lunine, J. I., McKay, C. P., Moussas, X., Müller-Wodarg, I., Neubauer, F., Owen, T. C., Raulin, F., Sittler, E. C., Sohl, F., Sotin, C., Tobie, G., Tokano, T., Turtle, E. P., Wahlund, J. E., Waite, J. H., Baines, K. H., Blamont, J., Coates, A. J., Dandouras, I., Krimigis, T., Lellouch, E., Lorenz, R. D., Morse, A., Porco, C. C., Hirtzig, M., Saur, J., Spilker, T., Zarnecki, J. C., Choi, E., Achilleos, N., Amils, R., Annan, P., Atkinson, D. H., Bénilan, Y., Bertucci, C., Bézard, B., Bjoraker, G. L., Blanc, M., Boireau, L., Bouman, J., Cabane, M., Capria, M. T., Chassefière, E., Coll, P., Combes, M., Cooper, J. F., Coradini, A., Crary, F., Cravens, T., Daglis, I. A., de Angelis, E., de Bergh, C., de Pater, I., Dunford, C., Durry, G., Dutuit, O., Fairbrother, D., Flasar, F. M., Fortes, A. D., Frampton, R., Fujimoto, M., Galand, M., Grasset, O., Grott, M., Haltigin, T., Herique, A.,

Hersant, F., Hussmann, H., Ip, W., Johnson, R., Kallio, E., Kempf, S., Knapmeyer, M., Kofman, W., Koop, R., Kostiuk, T., Krupp, N., Küppers, M., Lammer, H., Lara, L. M., Lavvas, P., Le Mouélic, S., Lebonnois, S., Ledvina, S., Li, J., Livengood, T. A., Lopes, R. M., Lopez-Moreno, J. J., Luz, D., Mahaffy, P. R., Mall, U., Martinez-Frias, J., Marty, B., McCord, T., Menor Salvan, C., Milillo, A., Mitchell, D. G., Modolo, R., Mousis, O., Nakamura, M., Neish, C. D., Nixon, C. A., Nna Mvondo, D., Orton, G., Paetzold, M., Pitman, J., Pogrebenko, S., Pollard, W., Prieto-Ballesteros, O., Rannou, P., Reh, K., Richter, L., Robb, F. T., Rodrigo, R., Rodriguez, S., Romani, P., Ruiz Bermejo, M., Sarris, E. T., Schenk, P., Schmitt, B., Schmitz, N., Schulze-Makuch, D., Schwingenschuh, K., Selig, A., Sicardy, B., Soderblom, L., Spilker, L. J., Stam, D., Steele, A., Stephan, K., Strobel, D. F., Szego, K., Szopa, C., Thissen, R., Tomasko, M. G., Toublanc, D., Vali, H., Vardavas, I., Vuitton, V., West, R. A., Yelle, R., Young, E. F., 2009. TandEM: Titan and Enceladus mission. Experimental Astronomy 23 (3), 893–946.

Coustenis, A., Jennings, D., Jolly, A., Bénilan, Y., Nixon, C., Vinatier, S., Gautier, D., Bjoraker, G., Romani, P., Carlson, R., Flasar, F., 2008. Detection of C_2HD and the D/H ratio on Titan. Icarus 197, 539–548.

Coustenis, A., Jennings, D. E., Achterberg, R. K., Lavvas, P., Bampasidis, G., Nixon, C. A., Flasar, F. M., 2020. Titan's neutral atmosphere seasonal variations up to the end of the Cassini mission. Icarus 344, 113413.

Coustenis, A., Nixon, C., Achterberg, R., Lavvas, P., Vinatier, S., Teanby, N., Bjoraker, G., Carlson, R., Piani, L., Bampasidis, G., Flasar, F., Romani, P., 2010. Titan trace gaseous composition from CIRS at the end of the Cassini-Huygens prime mission. Icarus 207, 461–476.

Coustenis, A., Salama, A., Lellouch, E., Encrenaz, T., Bjoraker, G., Samuelson, R., de Graauw, T., Feuchtgruber, H., Kessler, M., 1998. Evidence for water vapor in Titan's atmosphere from ISO/SWS data. Astron. Astrophys. 336, L85–L89.

Coustenis, A., Salama, A., Schulz, B., Ott, S., Lellouch, E., Encrenaz, T., Gautier, D., Feuchtgruber, H., 2003. Titan's atmosphere from ISO mid-infrared spectroscopy. Icarus 161 (2), 383–403.

Coutelier, M., Cordier, D., Seignovert, B., Rannou, P., Le Gall, A., Cours, T., Maltagliati, L., Rodriguez, S., Aug. 2021. Distribution and intensity of water ice signature in South Xanadu and Tui Regio. Icarus 364, 114464.

Couturier-Tamburelli, I., Piétri, N., Le Letty, V., Chiavassa, T., Gudipati, M., Jan. 2018a. UV-Vis Light-induced Aging of Titan's Haze and Ice. 852 (2), 117.

Couturier-Tamburelli, I., Toumi, A., Piétri, N., Chiavassa, T., Jan. 2018b. Behaviour of solid phase ethyl cyanide in simulated conditions of Titan. 300, 477–485.

Crary, F., Magee, B., Mandt, K., Waite Jr., J., Westlake, J., Young, D., 2009. Heavy ions, temperatures and winds in Titan's ionosphere: Combined Cassini CAPS and INMS observations. Planet. Space Sci. 57, 1847–1856.

Cravens, T., Robertson, I., Ledvina, S., Mitchell, D., Krimigis, S., Waite Jr., J., 2008. Energetic ion precipitation at Titan. Geophys. Res. Lett. 35, L03103.

Cravens, T., Robertson, I., Waite Jr., J., Yelle, R., Kasprzak, W., Keller, C., Ledvina, S., Niemann, H., Luhmann, J., McNutt Jr., R., Ip, W.-H., De La Haye, V., Müller-Wodarg, I., Wahlund, J.-E., Anicich, V., Vuitton, V., 2006. Composition of Titan's ionosphere. Geophys. Res. Lett. 33, L07105.

Cui, J., Galand, M., Yelle, R., Vuitton, V., Wahlund, J.-E., Lavvas, P., Müller-Wodarg, I., Cravens, T., Kasprzak, W., Waite, J., 2009a. Diurnal variations of Titan's ionosphere. J. Geophys. Res. 114, A06310.

Cui, J., Yelle, R., Vuitton, V., Waite, J., Kasprzak, W., Gell, D., Niemann, H., Müller-Wodarg, I., Borggren, N., Fletcher, G., Patrick, E., Raaen, E., Magee, B., 2009b. Analysis of Titan's neutral upper atmosphere from Cassini Ion Neutral Mass Spectrometer measurements. Icarus 200, 581–615.

Curtis, D., Hatch, C., Hasenkopf, C., Toon, O., Tolbert, M., McKay, C., Khare, B., 2008. Laboratory studies of methane and ethane adsorption and nucleation onto organic particles: Application to Titan's clouds. Icarus 195, 792–801.

de Kok, R., Irwin, P. G. J., Teanby, N. A., 2008. Condensation in Titan's stratosphere during polar winter. Icarus 197, 572–578.

de Kok, R., Irwin, P. G. J., Teanby, N. A., Lellouch, E., Bezard, B., Vinatier, S., Nixon, C. A., Fletcher, L., Howett, C., Calcutt, S. B., Bowles, N. E., Flasar, F. M., Taylor, F. W., 2007a. Oxygen compounds in Titan's stratosphere as observed by Cassini CIRS. Icarus 186, 354–363.

de Kok, R., Irwin, P. G. J., Teanby, N. A., Nixon, C. A., Jennings, D. E., Fletcher, L., Howett, C., Calcutt, S. B., Bowles, N. E., Flasar, F. M., Taylor, F. W., 2007b. Characteristics of Titan's stratospheric aerosols and condensate clouds from Cassini CIRS far-infrared spectra. Icarus 191, 223–235.

de Kok, R., Irwin, P. G. J., Teanby, N. A., Vinatier, S., Negrão, A., Osprey, S., Adriani, A., Moriconi, M. L., A., C., 2010. A tropical haze band in Titan's stratosphere. Icarus 207, 485–490.

de Kok, R. J., Teanby, N. A., Maltagliati, L., Irwin, P. G. J., Vinatier, S., 2014. HCN ice in Titan's high-altitude southern polar cloud. Nature 514, 65–67.

De La Haye, V., Waite Jr., J., Johnson, R., Yelle, R., Cravens, T., Luhmann, J., Kasprzak, W., Gell, D., Magee, B., Leblanc, F., Michael, M., Jurac, S., Robertson, I., 2007. Cassini Ion and Neutral Mass Spectrometer data in Titan's upper atmosphere and exosphere: Observation of a suprathermal corona. J. Geophys. Res. 112, A07309.

Desai, R. T., Coates, A. J., Wellbrock, A., Vuitton, V., Crary, F. J., González-Caniulef, D., Shebanits, O., Jones, G. H., Lewis, G. R., Waite, J. H., Cordiner, M., Taylor, S. A., Kataria, D. O., Wahlund, J.-E., Edberg, N. J. T., Sittler, E. C., Jul. 2017. Carbon Chain Anions and the Growth of Complex Organic Molecules in Titan's Ionosphere. The Astrophysical Journal 844 (2), L18.

Dimitrov, V., Bar-Nun, A., 2002. Aging of Titan's aerosols. Icarus 156 (2), 530–538.

Dinelli, B. M., López-Puertas, M., Adriani, A., Moriconi, M. L., Funke, B., García-Comas, M., D'Aversa, E., Apr. 2013. An unidentified emission in Titan's upper atmosphere. Geophysical Research Letters 40 (8), 1489–1493.

Dobrijevic, M., Hébrard, E., Loison, J., Hickson, K., 2014. Coupling of oxygen, nitrogen, and hydrocarbon species in the photochemistry of Titan's atmosphere. Icarus 228, 324–346.

Dobrijevic, M., Loison, J., Jun. 2018. The photochemical fractionation of nitrogen isotopologues in Titan's atmosphere. Icarus 307, 371–379.

Dobrijevic, M., Loison, J., Hickson, K., Gronoff, G., 2016. 1D-coupled photochemical model of neutrals, cations and anions in the atmosphere of Titan. Icarus 268, 313–339.

Doose, L., Karkoschka, E., Tomasko, M., Anderson, C., 2016. Vertical structure and optical properties of Titan's aerosols from radiance measurements made inside and outside the atmosphere. Icarus 270, 355–375.

Dubois, D., Carrasco, N., Bourgalais, J., Vettier, L., Desai, R. T., Wellbrock, A., Coates, A. J., Feb. 2019a. Nitrogen-containing Anions and Tholin Growth in Titan's Ionosphere: Implications for Cassini CAPS-ELS Observations. 872 (2), L31.

Dubois, D., Carrasco, N., Jovanovic, L., Vettier, L., Gautier, T., Westlake, J., Mar. 2020. Positive ion chemistry in an N_2-CH_4 plasma discharge: Key precursors to the growth of Titan tholins. 338, 113437.

Dubois, D., Carrasco, N., Petrucciani, M., Vettier, L., Tigrine, S., Pernot, P., Jan. 2019b. In situ investigation of neutrals involved in the formation of Titan tholins. 317, 182–196.

Dubois, D., Iraci, L. T., Barth, E. L., Salama, F., Vinatier, S., Sciamma-O'Brien, E., Jul. 2021. Investigating the Condensation of Benzene. The Planetary Science Journal 2 (4), 0–0.

Ennis, C., Cable, M. L., Hodyss, R., Maynard-Casely, H. E., Jul. 2020. Mixed Hydrocarbon and Cyanide Ice Compositions for Titan's Atmospheric Aerosols: A Ternary-Phase Cocrystal Predicted by Density Functional Theory. ACS Earth and Space Chemistry 4 (7), 1195–1200.

Fan, S., Shemansky, D. E., Li, C., Gao, P., Wan, L., Yung, Y. L., Aug. 2019. Retrieval of Chemical Abundances in Titan's Upper Atmosphere From Cassini UVIS Observations With Pointing Motion. Earth and Space Science 6 (7), 1057–1066.

Flasar, F. M., Achterberg, R. K., Conrath, B. J., Gierasch, P. J., Kunde, V. G., Nixon, C. A., Bjoraker, G. L., Jennings, D. E., Romani, P. N., Simon-Miller, A. A., Bézard, B., Coustenis, A., Irwin, P. G. J., Teanby, N. A., Brasunas, J., Pearl, J. C., Segura, M. E., Carlson, R. C., Mamoutkine, A., Schinder, P. J., Barucci, A., Courtin, R., Fouchet, T., Gautier, D., Lellouch, E., Marten, A., Prange, R., Vinatier, S., Strobel, D. F., Calcutt, S. B., Read, P. L., Taylor, F. W., Bowles, N., Samuelson, R. E., Orton, G. S., Spilker, L. J., Owen, T. C., Spencer, J. R., Showalter, M. R., Ferrari, C., Abbas, M. M., Raulin, F., Edgington, S., Ade, P., Wishnow, E. H., 2005. Titan's atmospheric temperatures, winds, and composition. Science 308, 975–978.

Flasar, F. M., Baines, K. H., Bird, M. K., Tokano, T., West, R. A., 2010. Atmospheric Dynamics and Meteorology. In: Brown, R. H., Lebreton, J.-P., Waite, J. H. (Eds.), Titan from Cassini-Huygens. pp. 323–352.

Fleury, B., Gudipati, M. S., Couturier-Tamburelli, I., Carrasco, N., Mar. 2019. Photoreactivity of condensed acetylene on Titan aerosols analogues. 321, 358–366.

Fulchignoni, M., Ferri, F., Angrilli, F., Ball, A. J., Bar-Nun, A., Barucci, M. A., Bettanini, C., Bianchini, G., Borucki, W., Colombatti, G., Coradini, M., Coustenis, A., Debei, S., Falkner, P., Fanti, G., Flamini, E., Gaborit, V., Grard, R., Hamelin, M., Harri, A. M., Hathi, B., Jernej, I., Leese, M. R., Lehto, A., Stoppato, P. F. L., Lopez-Moreno, J. J., Makinen, T., McDonnell, J. A. M., McKay, C. P., Molina-Cuberos, G., Neubauer, F. M., Pirronello, V., Rodrigo, R., Saggin, B., Schwingenschuh, K., Seiff, A., Simoes, F., Svedhem, H., Tokano, T., Towner, M. C., Trautner, R., Withers, P., Zarnecki, J. C., 2005. In situ measurements of the physical characteristics of Titan's environment. Nature 438, 785–791.

Galand, M., Yelle, R., Cui, J., Wahlund, J.-E., Vuitton, V., Wellbrock, A., Coates, A., 2010. Ionization sources in Titan's deep ionosphere. J. Geophys. Res. 115, A07312.

García Muñoz, A., Lavvas, P., West, R. A., Apr. 2017. Titan brighter at twilight than in daylight. Nature Astronomy 1 (5), 0114.

Gavilan, L., Carrasco, N., Hoffmann, S. V., Jones, N. C., Mason, N. J., Jul. 2018. Organic Aerosols in Anoxic and Oxic Atmospheres of Earth-like Exoplanets: VUV-MIR Spectroscopy of CHON Tholins. The Astrophysical Journal 861 (2), 110.

Griffith, C., Penteado, P., Baines, K., Drossart, P., Barnes, J., Bellucci, G., Bibring, J., Brown, R., Buratti, B., Capaccioni, F., Cerroni, P., Clark, R., Combes, M., Coradini, A., Cruikshank, D., Formisano, V., Jaumann, R., Langevin, Y., Matson, D., McCord, T., Mennella, V., Nelson, R., Nicholson, P., Sicardy, B., Sotin, C., Soderblom, L., Kursinski, R., Oct. 2005. The evolution of Titan's mid-latitude clouds. Science 310, 474–477.

Griffith, C.-A., Penteado, P., Rannou, P., Brown, R., Boudon, V., Baines, K.-H., Clark, R., Drossart, P., Buratti, B., Nicholson, P., McKay, C.-P., Coustenis, A., Negrao, A., Jaumann, R., Sep. 2006. Evidence for a Polar Ethane Cloud on Titan. Science 313, 1620–1622.

Gronoff, G., Lilensten, J., Modolo, R., 2009. Ionization processes in the atmosphere of Titan II. Electron precipitation along magnetic field lines. Astron. Astrophys. 506, 965–970.

Gronoff, G., Mertens, C., Lilensten, J., Desorgher, L., Flückiger, E., Velinov, P., 2011. Ionization processes in the atmosphere of Titan III. Ionization by high-Z nuclei cosmic rays. Astron. Astrophys. 529, A143.

Hamelin, M., Béghin, C., Grard, R., López-Moreno, J., Schwingenschuh, K., Sim\-oes, F., Trautner, R., Berthelier, J., Brown, V., Chabassière, M., Falkner, P., Ferri, F., Fulchignoni, M., Jernej, I., Jeronimo, J., Molina-Cuberos, G., Rodrigo, R., Tokano, T., 2007. Electron conductivity and density profiles derived from the mutual impedance probe measurements performed during the descent of Huygens through the atmosphere of Titan. Planet. Space Sci. 55, 1964–1977.

Hartogh, P., Lellouch, E., Moreno, R., Bockelée-Morvan, D., Biver, N., Cassidy, T., Rengel, M., Jarchow, C., Cavalié, T., Crovisier, J., Helmich, F., Kidger, M., 2011. Direct detection of the Enceladus water torus with $Herschel$. Astron. Astrophys. 532 (L2).

Haythornthwaite, R. P., Coates, A. J., Jones, G. H., Wellbrock, A., Waite, J. H., Vuitton, V., Lavvas, P., Feb. 2021. Heavy Positive Ion Groups in Titan's Ionosphere from Cassini Plasma Spectrometer IBS Observations. The Planetary Science Journal 2 (1), 26.

Hewett, D., Bernath, P. F., Wong, A., Billinghurst, B. E., Zhao, J., Lombardo, N. A., Nixon, C. A., Jennings, D. E., Jul. 2020. N_2 and H_2 broadened isobutane infrared absorption cross sections and butane upper limits on Titan. 344, 113460.

Hong, P., Sekine, Y., Sasamori, T., Sugita, S., Jun. 2018. Experimental study of heterogeneous organic chemistry induced by far ultraviolet light: Implications for growth of organic aerosols by CH_3 addition in the atmospheres of Titan and early Earth. 307, 25–39.

Hörst, S., Vuitton, V., Yelle, R., 2008. The origin of oxygen species in Titan's atmosphere. J. Geophys. Res. 113, E10006.

Hörst, S. M., 2017. Titan's atmosphere and climate. J. Geophys. Res. Planets 122, doi:10.1002/2016JE005240.

Hörst, S. M., He, C., Lewis, N. K., Kempton, E. M. R., Marley, M. S., Morley, C. V., Moses, J. I., Valenti, J. A., Vuitton, V., Apr. 2018. Haze production rates in super-Earth and mini-Neptune atmosphere experiments. Nature Astronomy 2, 303–306.

Horvath, G., Aranda-Gonzalvo, Y., Mason, N., Zahoran, M., Matejcik, S., 2010. Negative ions formed in N2/CH4/Ar discharge - A simulation of Titan's atmosphere chemistry. Eur. Phys. J. Appl. Phys. 49, 13105.

Hourdin, F., Talagrand, O., Sadourny, R., Courtin, R., Gautier, D., McKay, C., 1995. Numerical simulation of the general circulation of the atmosphere of Titan. Icarus 117, 358–374.

Hubbard, W. B., Sicardy, B., Miles, R., Hollis, A. J., Forrest, R. W., Nicolson, I. K. M., Appleby, G., Beisker, W., Bittner, C., Bode, H. J., Bruns, M., Denzau, H., Nezel, M., Riedel, E., Struckmann, H., Arlot, J. E., Roques, F., Sevre, F., Thuillot, W., Hoffmann, M., Geyer, E. H., Buil, C., Colas, F., Lecacheux, J., Klotz, A., Thouvenot, E., Vidal, J. L., Carreira, E., Rossi, F., Blanco, C., Cristaldi, S., Nevo, Y., Reitsema, H. J., Brosch, N., Cernis, K., Zdanavicius, K., Wasserman, L. H., Hunten, D. M., Gautier, D., Lellouch, E., Yelle, R. V., Rizk, B., Flasar, F. M., Porco, C. C., Toublanc, D., Corugedo, G., 1993. The occultation of 28-Sgr by Titan. Astron. Astrophys. 269, 541–563.

Iino, T., Sagawa, H., Tsukagoshi, T., Feb. 2020. $^{14}N/^{15}N$ Isotopic Ratio in CH_3CN of Titan's Atmosphere Measured with ALMA. 890 (2), 95.

Imanaka, H., Khare, B.-N., Elsila, J.-E., Bakes, E.-L.-O., McKay, C.-P., Cruikshank, D.-P., Sugita, S., Matsui, T., Zare, R.-N., Apr. 2004. Laboratory experiments of Titan tholin formed in cold plasma at various pressures: implications for nitrogen-containing polycyclic aromatic compounds in Titan haze. Icarus 168, 344–366.

Imanaka, H., Smith, M.-A., Jul. 2010. Formation of nitrogenated organic aerosols in the Titan Upper Atmosphere. PNAS 28, 12423–12428.

Israël, G., Szopa, C., Raulin, F., Cabane, M., Niemann, H., Atreya, S., Bauer, S., Brun, J.-F., Chassefière, E., Coll, P., Condé, E., Coscia, D., Hauchecorne, A., Millian, P., Nguyen, M.-J., Owen, T., Riedler, W., Samuelson, R., Siguier, J.-M., Steller, M., Sternberg, R., Vidal-Madjar, C., 2005. Complex organic matter in Titan's atmospheric aerosols from in situ pyrolysis and analysis. Nature 438, 796–799.

Jennings, D., Nixon, C., Jolly, A., Bézard, B., Coustenis, A., Vinatier, S., Irwin, P., Teanby, N., Romani, P., Achterberg, R., Flasar, F., 2008. Isotopic ratios in Titan's atmosphere from Cassini CIRS limb sounding: HC3N in the North. Astrophys. J. 681, L109–L111.

Jolly, A., Cottini, V., Fayt, A., Manceron, L., Kwabia-Tchana, F., Benilan, Y., Guillemin, J. C., Nixon, C., Irwin, P., Mar. 2015. Gas phase dicyanoacetylene (C_4N_2) on Titan: New experimental and theoretical spectroscopy results applied to Cassini CIRS data. 248, 340–346.

Jolly, A., Fayt, A., Benilan, Y., Jacquemart, D., Nixon, C. A., Jennings, D. E., May 2010. The ν_8 Bending Mode of Diacetylene: From Laboratory Spectroscopy to the Detection of ^{13}C Isotopologues in Titan's Atmosphere. 714 (1), 852–859.

Karkoschka, E., Nov. 2022. Titan's haze at opposite seasons from HST-STIS spectroscopy. Icarus 387, 115188.

Khare, B., Sagan, C., Arakawa, E., Suits, F., Callcott, A., Williams, M., 1984. Optical constants of organic tholins produced in a simulated Titanian atmosphere: from soft X-ray to microwave frequencies. Icarus 60 (1), 127–137.

Khlifi, M., Paillous, P., Bruston, P., Raulin, F., Guillemin, J.-C., Nov. 1996. Absolute IR band intensities of CH_2N_2, CH_3N_3, and CH_3NC in the 250-4300 cm$^{-1\$}$ region and upper limits of abundance in Titan's stratosphere. Icarus 124, 318–328.

Koskinen, T., Yelle, R., Snowden, D., Lavvas, P., Sandel, B., Capalbo, F., Bénilan, Y., West, R., 2011. The mesosphere and thermosphere of Titan revealed by Cassini/UVIS stellar occultations. Icarus 216, 507–534.

Lacy, J., Richter, M., Greathouse, T., Jaffe, D., Zhu, Q., 2002. Texes: A sensitive high-resolution grating spectrograph for the mid-infrared. Publications of the Astronomical Society of the Pacific 114 (792), 153.

Larson, E. J. L., Feb. 2019. Seasonal Changes in Titan. The Astrophysical Journal Letters 872 (2), 0–0.

Larson, E. J. L., Toon, O. B., Friedson, A. J., Nov. 2014. Simulating Titan's aerosols in a three dimensional general circulation model. Icarus 243, 400–419.

Lavvas, P., Coustenis, A., Vardavas, I., 2008. Coupling photochemistry with haze formation in Titan's atmosphere. Part II: Results and validation with Cassini/Huygens data. Planet. Space Sci. 56, 67–99.

Lavvas, P., Galand, M., Yelle, R., Heays, A., Lewis, B., Lewis, G., Coates, A., 2011a. Energy deposition and primary chemical products in Titan's upper atmosphere. Icarus 213, 233–251.

Lavvas, P., Griffith, C., Yelle, R., 2011b. Condensation in Titan's atmosphere at the Huygens landing site. Icarus 215, 732–750.

Lavvas, P., Sander, M., Kraft, M., Imanaka, H., 2011c. Surface chemistry and particle shape. Processes for the evolution of aerosols in Titan's atmosphere. Astrophys. J. 728, 80–90.

Lavvas, P., Yelle, R., Griffith, C., 2010. Titan's vertical aerosol structure at the Huygens landing site: Constraints on particle size, density, charge, and refractive index. Icarus 210, 832–842.

Lavvas, P., Yelle, R., Koskinen, T., Bazin, A., Vuitton, V., Vigren, E., Galand, M., Wellbrock, A., Coates, A., Wahlund, J.-E., Crary, F., Snowden, D., 2013. Aerosol growth in Titan's ionosphere. PNAS 110, 2729–2734.

Lavvas, P., Yelle, R., Vuitton, V., 2009. The detached haze layer in Titan's mesosphere. Icarus 201, 626–633.

Lebonnois, S., Burgalat, J., Rannou, P., Charnay, B., 2012. Titan global climate model: a new 3-dimensional version of the IPSL Titan GCM. Icarus 218, 707–722.

Lebreton, J. P., Witasse, O., Sollazzo, C., Blancquaert, T., Couzin, P., Schipper, A. M., Jones, J. B., Matson, D. L., Gurvits, L. I., Atkinson, D. H., Kazeminejad, B., Perez-Ayucar, M., 2005. An overview of the descent and landing of the Huygens probe on Titan. Nature 438, 758–764.

Lellouch, E., Bézard, B., Flasar, F., Vinatier, S., Achterberg, R., Nixon, C., Bjoraker, G., Gorius, N., 2014. The distribution of methane in Titan's stratosphere from Cassini/CIRS observations. Icarus 231, 323–337.

Lellouch, E., Bézard, B., Flasar, F. M., Vinatier, S., Achterberg, R., Nixon, C. A., Bjoraker, G. L., Gorius, N., 2014. The distribution of methane in Titan's stratosphere from Cassini/CIRS observations. Icarus 231, 323–337.

Lellouch, E., Gurwell, M. A., Moreno, R., Vinatier, S., Strobel, D. F., Moullet, A., Butler, B., Lara, L., Hidayat, T., Villard, E., 2019. An intense thermospheric jet on Titan. Nature Astronomy 3, 614–619.

Li, L., Nixon, C. A., Achterberg, R. K., Smith, M. A., Gorius, N. J. P., Jiang, X., Conrath, B. J., Gierasch, P. J., Simon-Miller, A. A., Flasar, F. M., Baines, K. H., Ingersoll, A. P., West, R. A., Vasavada, A. R., Ewald, S. P., 2011. The global energy balance of Titan. Geophys. Res. Lett. 38, L23201.

Liang, M.-C., Yung, Y.-L., Shemansky, D.-E., Jun. 2007. Photolytically Generated Aerosols in the Mesosphere and Thermosphere of Titan. ApJL 661, L199–L202.

Loison, J., Dobrijevic, M., Hickson, K., Sep. 2019. The photochemical production of aromatics in the atmosphere of Titan. Icarus 329, 55–71.

Loison, J., Hébrard, E., Dobrijevic, M., Hickson, K., Caralp, F., Hue, V., Gronoff, G., Venot, O., Benilan, Y., 2015. The neutral photochemistry of nitriles, amines and imines in the atmosphere of Titan. Icarus 247, 218–247.

Lombardo, N. A., Lora, J. M., 2022. Influence of observed seasonally varying composition on titan's stratospheric circulation. Icarus, 115291.

Lombardo, N. A., Nixon, C. A., Achterberg, R. K., Jolly, A., Sung, K., Irwin, P. G. J., Flasar, F. M., Jan. 2019a. Spatial and seasonal variations in C_3H_x hydrocarbon abundance in Titan's stratosphere from Cassini CIRS observations. 317, 454–469.

Lombardo, N. A., Nixon, C. A., Greathouse, T. K., Bézard, B., Jolly, A., Vinatier, S., Teanby, N. A., Richter, M. J., Irwin, P. J. G., Coustenis, A., Flasar, F. M., 2019b. Detection of Propadiene on Titan. 881 (2), L33.

López-Moreno, J., Molina-Cuberos, G., Hamelin, M., Grard, R., Sim\-oes, F., Godard, R., Schwingenschuh, K., Béghin, C., Berthelier, J., Brown, V., Falkner, P., Ferri, F., Fulchignoni, M., Jernej, I., Jerónimo, J., Rodrigo, R., Trautner, R., 2008. Structure of Titan's low altitude ionized layer from the Relaxation Probe onboard HUYGENS. Geophys. Res. Lett. 35, L22104.

López-Puertas, M., Dinelli, B. M., Adriani, A., Funke, B., García-Comas, M., Moriconi, M. L., D'Aversa, E., Boersma, C., Allamandola, L. J., Jun. 2013. Large abundances of polycyclic aromatic hydrocarbons in Titan's upper atmosphere. The Astrophysical Journal 770 (2), 132.

Lorenz, R. D., Young, L. A., Ferri, F., 2014. Gravity waves in Titan's lower stratosphere from Huygens probe in situ temperature measurements. Icarus 227, 49–55.

Lutz, B.-L., de Bergh, C., Owen, T., Jun. 1983. Titan - Discovery of carbon monoxide in its atmosphere. Science 220, 1374–+.

Luz, D., Hourdin, F., Rannou, P., Lebonnois, S., 2003. Latitudinal transport by barotropic waves in Titan's stratosphere. II. Results from a coupled dynamics-microphysics-photochemistry GCM. Icarus 166, 343–358.

Magee, B., Waite, J., Mandt, K., Westlake, J., Bell, J., Gell, D., 2009. INMS-derived composition of Titan's upper atmosphere: Analysis methods and model comparison. Planet. Space Sci. 57, 1895–1916.

Mahjoub, A., Schwell, M., Carrasco, N., Benilan, Y., Cernogora, G., Szopa, C., Gazeau, M.-C., Oct. 2016. Characterization of aromaticity in analogues of titan's atmospheric aerosols with two-step laser desorption ionization mass spectrometry. 131, 1–13.

Maillard, J., Hupin, S., Carrasco, N., Schmitz-Afonso, I., Gautier, T., Afonso, C., Apr. 2020. Structural elucidation of soluble organic matter: Application to Titan's haze. 340, 113627.

Maltagliati, L., Bézard, B., Vinatier, S.and Hedman, M., Lellouch, E., Nicholson, P., Sotin, C., de Kok, R., Sicardy, B., 2015. Titan's atmosphere as observed by Cassini/VIMS solar occultations: \ceCH4, CO and evidence for \ceC2H6 absorption. Icarus 248, 1–24.

Marten, A., Hidayat, T., Biraud, Y., Moreno, R., 2002. New millimeter heterodyne observations of Titan: Vertical distributions of HCN HC_3N, CH_3CN, and the isotopic ratio $^{15\$}N/^{14\$}N$ in its atmosphere. Icarus 158, 532 – 544.

Mathé, C., Vinatier, S., Bézard, B., Lebonnois, S., Gorius, N., Jennings, D. E., Mamoutkine, A., Guandique, E., Vatant d'Ollone, J., 2020. Seasonal changes in the middle atmosphere of Titan from Cassini/CIRS observations: Temperature and trace species abundance profiles from 2004 to 2017. Icarus 344, 113547.

Michael, M., Tripathi, S., Arya, P., Coates, A., Wellbrock, A., Young, D., 2011. High-altitude charged aerosols in the atmosphere of Titan. Planet. Space Sci. 59, 880–885.

Mihailescu, T., Desai, R. T., Shebanits, O., Haythornthwaite, R., Wellbrock, A., Coates, A. J., Eastwood, J. P., Waite, J. H., Sep. 2020. Spatial Variations of Low-mass Negative Ions in Titan's Upper Atmosphere. 1 (2), 50.

Mitchell, D. M., Scott, R. K., Seviour, W. J. M., Thomson, S. I., Waugh, D. W., Teanby, N. A., Ball, E. R., 2021. Polar Vortices in Planetary Atmospheres. Rev. Geophys. 59 (4), e00723.

Mitri, G., Postberg, F., Soderblom, J. M., Wurz, P., Tortora, P., Abel, B., Barnes, J. W., Berga, M., Carrasco, N., Coustenis, A., Paul de Vera, J. P., D'Ottavio, A., Ferri, F., Hayes, A. G., Hayne, P. O., Hillier, J. K., Kempf, S., Lebreton, J.-P., Lorenz, R. D., Martelli, A., Orosei, R., Petropoulos, A. E., Reh, K., Schmidt, J., Sotin, C., Srama, R., Tobie, G., Vorburger, A., Vuitton, V., Wong, A., Zannoni, M., 2018. Explorer of Enceladus and Titan (E^2T): Investigating ocean worlds' evolution and habitability in the solar system. Plan. & Space Sci. 155, 73–90.

Molina-Cuberos, G., Lammer, H., Stumptner, W., Schwingenschuh, K., Rucker, H., López-Moreno, J., Rodrigo, R., Tokano, T., 2001. Ionospheric layer induced by meteoric ionization in Titan's atmosphere. Planet. Space Sci. 49, 143–153.

Molina-Cuberos, G. J., Cardnell, S., García-Collado, A. J., Witasse, O., López-Moreno, J. J., Apr. 2018. Aerosols: The key to understanding Titan's lower ionosphere. 153, 157–162.

Molina-Cuberos, G. J., López-Moreno, J. J., Rodrigo, R., Lara, L. M., O'Brien, K., 1999. Ionization by cosmic rays of the atmosphere of Titan. Planet. Space Sci. 47 (10-11), 1347–1354.

Molter, E. M., Nixon, C. A., Cordiner, M. A., Serigano, J., Irwin, P. G. J., Teanby, N. A., Charnley, S. B., Lindberg, J. E., Aug. 2016. ALMA Observations of HCN and Its Isotopologues on Titan. 152 (2), 42.

Moreno, R., Lellouch, E., Lara, L., Feuchtgruber, H., Rengel, M., Hartogh, P., Courtin, R., 2012. The abundance, vertical distribution and origin of \ceH2O in Titan's atmosphere: Herschel observations and photochemical modelling. Icarus 221, 753–767.

Morgan, N., Kraft, M., Balthasar, M., Wong, D., Frenklach, M., Mitchell, P., Jan. 2007. Numerical simulations of soot aggregation in premixed laminar flames. Proceedings Of The Combustion Institute 31 (1), 693–700.

Mousis, O., Gautier, D., Bockelée-Morvan, D., Mar. 2002. An Evolutionary Turbulent Model of Saturn's Subnebula: Implications for the Origin of the Atmosphere of Titan. Icarus 156, 162–175.

Mousis, O., Gautier, D., Coustenis, A., Sep. 2002. The D/H Ratio in Methane in Titan: Origin and History. 159 (1), 156–165.

Mouzay, J., Henry, K., Couturier-Tamburelli, I., Danger, G., Piétri, N., Chiavassa, T., Nov. 2021a. Photochemistry of benzene (C_6H_6) hydrogen cyanide (HCN) co-condensed ices part 1: A source of solid-state production of volatile nitrile compounds in Titan's stratosphere. 368, 114595.

Mouzay, J., Henry, K., Ruf, A., Couturier-Tamburelli, I., Danger, G., Piétri, N., Chiavassa, T., Feb. 2021b. Experimental Simulation of the Volatile Hydrocarbons Generated by the Long-UV Photoprocessing of (C_6H_6) Ices with Relevance to Titan's Southern Stratospheric Ice Clouds. 2 (1), 37.

Mukundan, V., Bhardwaj, A., Apr. 2018. A Model for Negative Ion Chemistry in Titan's Ionosphere. 856 (2), 168.

Muller-Wodarg, I. C. F., Yelle, R. V., Borggren, N., Waite, J. H., 2006. Waves and horizontal structures in Titan's thermosphere. J. Geophys. Res. 111.

Newman, C. E., Lee, C., Lian, Y., Richardson, M. I., Toigo, A. D., 2011. Stratospheric superrotation in the TitanWRF model. Icarus 213, 636–654.

Niemann, H., Atreya, S., Demick, J., Gautier, D., Haberman, J., Harpold, D., Kasprzak, W., Lunine, J., Owen, T., Raulin, F., 2010. Composition of Titan's lower atmosphere and simple surface volatiles as measured by the Cassini-Huygens probe gas chromatograph mass spectrometer experiment. J. Geophys. Res. 115, E12006.

Nixon, C., Achterberg, R., Teanby, N., Irwin, P., Flaud, J.-M., Kleiner, I., Dehayem-Kamadjeu, A., Brown, L., Sams, R., Bézard, B., Coustenis, A., Ansty, T., Mamoutkine, A., Vinatier, S., Bjoraker, G., Jennings, D., Romani, P., Flasar, F., 2010. Upper limits for undetected trace species in the stratosphere of Titan. Faraday Discuss. 147, 65–81.

Nixon, C., Jennings, D., Flaud, J.-M., Bézard, B., Teanby, N., Irwin, P., Ansty, T., Coustenis, A., Vinatier, S., Flasar, F., 2009. Titan's prolific propane: The Cassini CIRS perspective. Planet. Space Sci. 57, 1573–1585.

Nixon, C. A., Achterberg, R. K., Ádámkovics, M., Bézard, B., Bjoraker, G. L., Cornet, T., Hayes, A. G., Lellouch, E., Lemmon, M. T., López-Puertas, M., Rodriguez, S., Sotin, C., Teanby, N. A., Turtle, E. P., West, R. A., 2016. Titan Science with the James Webb Space Telescope. Pub. Ast. Soc. Pacific 128 (959), 018007.

Nixon, C. A., Achterberg, R. K., Vinatier, S., Bézard, B., Coustenis, A., Irwin, P. G. J., Teanby, N. A., de Kok, R., Romani, P. N., Jennings, D. E., Bjoraker, G. L., Flasar, F. M., Jun. 2008a. The $^{12}C/\ ^{13}C$ isotopic ratio in Titan hydrocarbons from Cassini/CIRS infrared spectra. 195 (2), 778–791.

Nixon, C. A., Jennings, D. E., Bézard, B., Teanby, N. A., Achterberg, R. K., Coustenis, A., Vinatier, S., Irwin, P. G. J., Romani, P. N., Hewagama, T., Flasar, F. M., Jul. 2008b. Isotopic Ratios in Titan's Atmosphere from Cassini CIRS Limb Sounding: CO_2 at Low and Midlatitudes. 681 (2), L101.

Nixon, C. A., Lorenz, R. D., Achterberg, R. K., Buch, A., Coll, P., Clark, R. N., Courtin, R., Hayes, A., Iess, L., Johnson, R. E., Lopes, R. M. C., Mastrogiuseppe, M., Mandt, K., Mitchell, D. G., Raulin, F., Rymer, A. M., Todd Smith, H., Solomonidou, A., Sotin, C., Strobel, D., Turtle, E. P., Vuitton, V., West, R. A., Yelle, R. V., 2018. Titan's cold case files - Outstanding questions after Cassini-Huygens. Plan. & Space Sci. 155, 50–72.

Nixon, C.-A., Teanby, N.-A., Irwin, P.-G.-J., Hörst, S.-M., May 2013. Upper limits for PH_3 and H_2S in Titan's atmosphere from Cassini CIRS. Icarus 224, 253–256.

Nixon, C. A., Temelso, B., Vinatier, S., Teanby, N., Bézard, B., Achterberg, R., Mandt, K., Sherrill, C., Irwin, P., Jennings, D., Romani, P., Coustenis, A., Flasar, F., 2012. Isotopic ratios in Titan's methane: Measurements and modeling. Astrophys. J. 749, 159.

Nixon, C. A., Thelen, A. E., Cordiner, M. A., Kisiel, Z., Charnley, S. B., Molter, E. M., Serigano, J., Irwin, P. G. J., Teanby, N. A., Kuan, Y.-J., Nov. 2020. Detection of Cyclopropenylidene on Titan with ALMA. 160 (5), 205.

Nna-Mvondo, D., Anderson, C. M., Feb. 2022. Infrared Spectra, Optical Constants, and Temperature Dependences of Amorphous and Crystalline Benzene Ices Relevant to Titan. The Astrophysical Journal 925 (2), 123.

Nna-Mvondo, D., Anderson, C. M., Samuelson, R. E., Nov. 2019. Detailed infrared study of amorphous to crystalline propionitrile ices relevant to observed spectra of Titan's stratospheric ice clouds. 333, 183–198.

Owen, T., Aug. 1982. The composition and origin of Titan's atmosphere. Planet. Space Sci. 30, 833–838.

Owen, T., Niemann, H., 2009. The origin of Titan's atmosphere: some recent advances. Phil. Trans. R. Soc. A 367, 607–615.

Palmer, M., Cordiner, M., Nixon, C., Charnley, S., Teanby, N., Kisiel, Z., Irwin, P., Mumma, M., 2017. ALMA detection and astrobiological potential of vinyl cyanide on Titan. Sci. Adv. 3 (e1700022).

Pierel, J. D. R., Nixon, C. A., Lellouch, E., Fletcher, L. N., Bjoraker, G. L., Achterberg, R. K., Bézard, B., Hesman, B. E., Irwin, P. G. J., Flasar, F. M., Nov. 2017. D/H Ratios on Saturn and Jupiter from Cassini CIRS. 154 (5), 178.

Porco, C.-C., Baker, E., Barbara, J., Beurle, K., Brahic, A., Burns, J.-A., Charnoz, S., Cooper, N., Dawson, D.-D., Del Genio, A.-D., Denk, T., Dones, L., Dyudina, U., Evans, M.-W., Fussner, S., Giese, B., Grazier, K., Helfenstein, P., Ingersoll, A.-P., Jacobson, R.-A., Johnson, T.-V., McEwen, A., Murray, C.-D., Neukum, G., Owen, W.-M., Perry, J., Roatsch, T., Spitale, J., Squyres, S., Thomas, P., Tiscareno, M., Turtle, E.-P., Vasavada, A.-R., Veverka, J., Wagner, R., West, R., Mar. 2005. Imaging of Titan from the Cassini spacecraft. Nature 434, 159–168.

Rannou, P., Cours, T., Le Mouélic, S., Rodriguez, S., Sotin, C., Drossart, P., Brown, R., 2010. Titan haze distribution and optical properties retrieved from recent observations. Icarus 208, 850–867.

Rannou, P., Coutelier, M., Rey, M. M., Vinatier, S., 2022. Analysis of four solar occultations by titan's atmosphere with the infrared instrument of vims: Haze, ch4, ch3d and co vertical profiles. Astronomy and Astrophysics-A&A 666, A140.

Rannou, P., Curtis, D., Tolbert, M. A., Nov. 2019. Adsorption isotherms and nucleation of methane and ethane on an analog of Titan's photochemical aerosols. Astronomy and Astrophysics 631, A151–12.

Rannou, P., Hourdin, F., McKay, C.-P., Aug. 2002. A wind origin for Titan's haze structure. Nature 418, 853–856.

Rannou, P., Hourdin, F., McKay, C.-P., Luz, D., Aug. 2004. A coupled dynamics-microphysics model of Titan's atmosphere. Icarus 170, 443–462.

Rannou, P., Montmessin, F., Hourdin, F., Lebonnois, S., 2006. The latitudinal distribution of clouds on Titan. Science 311, 201–205.

Raulin, F., Jan. 1990. Infrared spectra of gaseous organics: Application to the atmosphere of Titan—II. Infrared intensities and frequencies of C4 alkanenitriles and benzene. Spectrochimica Acta Part A: Molecular Spectroscopy 46 (5), 671–683.

Rey, M., Nikitin, A. V., Bézard, B., Rannou, P., Coustenis, A., Tyuterev, V. G., 2018. New accurate theoretical line lists of 12ch4 and 13ch4 in the 0–13400 cm- 1 range: Application to the modeling of methane absorption in titan's atmosphere. Icarus 303, 114–130.

Robertson, I., Cravens, T., Waite Jr., J., Yelle, R., Vuitton, V., Coates, A., Wahlund, J.-E., Ågren, K., Mandt, K., Magee, B., Richard, M., Fattig, E., 2009. Structure of Titan's ionosphere: Model comparisons with Cassini data. Planet. Space Sci. 57, 1834–1846.

Rodriguez, S., Le Mouélic, S., Rannou, P., Tobie, G., Baines, K., Barnes, J., Griffith, C., Hirtzig, M., Pitman, K., Sotin, C., Brown, R., Buratti, B., Clark, R., Nicholson, P., 2009. Global circulation as the main source of cloud activity on Titan. Nature 459, 678–682.

Rodriguez, S., Vinatier, S., Cordier, D., Tobie, G., Achterberg, R. K., Anderson, C. M., Badman, S. V., Barnes, J. W., Barth, E. L., Bézard, B., Carrasco, N., Charnay, B., Clark, R. N., Coll, P., Cornet, T., Coustenis, A., Couturier-Tamburelli, I., Dobrijevic, M., Flasar, F. M., de Kok, R., Freissinet, C., Galand, M., Gautier, T., Geppert, W. D., Griffith, C. A., Gudipati, M. S., Hadid, L. Z., Hayes, A. G., Hendrix, A. R., Jaumann, R., Jennings, D. E., Jolly, A., Kalousova, K., Koskinen, T. T., Lavvas, P., Lebonnois, S., Lebreton, J.-P., Le Gall, A., Lellouch, E., Le Mouélic, S., Lopes, R. M. C., Lora, J. M., Lorenz, R. D., Lucas, A., MacKenzie, S., Malaska, M. J., Mandt, K., Mastrogiuseppe, M., Newman, C. E., Nixon, C. A., Radebaugh, J., Rafkin, S. C., Rannou, P., Sciamma-O'Brien, E. M., Soderblom, J. M., Solomonidou, A., Sotin, C., Stephan, K., Strobel, D., Szopa, C., Teanby, N. A., Turtle, E. P., Vuitton, V., West, R. A., 2022. Science goals and new mission concepts for future exploration of Titan's atmosphere, geology and habitability: titan POlar scout/orbitEr and in situ lake lander and DrONe explorer (POSEIDON). Experimental Astronomy.

Roman, M. T., West, R. A., Banfield, D. J., Gierasch, P. J., Achterberg, R. K., Nixon, C. A., Thomas, P. C., 2009. Determining a tilt in Titan's north-south albedo asymmetry from Cassini images. Icarus 203, 242–249.

Sagnières, L., Galand, M., Cui, J., Lavvas, P., Vigren, E., Vuitton, V., Yelle, R., Wellbrock, A., Coates, A., 2015. Influence of local ionization on ionospheric densities in Titan's upper atmosphere. J. Geophys. Res. Space Physics 120.

Samuelson, R. E., Hanel, R. A., Kunde, V. G., Maguire, W. C., 1981. Mean molecular weight and hydrogen abundance of Titan's atmosphere. Nature 292, 688–693.

Schulz, F., Maillard, J., Kaiser, K., Schmitz-Afonso, I., Gautier, T., Afonso, C., Carrasco, N., Gross, L., Feb. 2021. Imaging Titan's Organic Haze at Atomic Scale. 908 (1), L13.

Scott, R. K., Seviour, W. J. M., Waugh, D. W., 2020. Forcing of the Martian polar annulus by Hadley cell transport and latent heating. Quart. J. Roy. Met. Soc. 146 (730), 2174–2190.

Seignovert, B., Rannou, P., Lavvas, P., Cours, T., West, R. A., Aug. 2017. Aerosols optical properties in Titan's detached haze layer before the equinox. Icarus 292, 13–21.

Serigano, J., Nixon, C. A., Cordiner, M. A., Irwin, P. G. J., Teanby, N. A., Charnley, S. B., Lindberg, J. E., Apr. 2016. Isotopic Ratios of Carbon and Oxygen in Titan's CO using ALMA. 821 (1), L8.

Sharkey, J., Teanby, N. A., Sylvestre, M., Mitchell, D. M., Seviour, W. J. M., Nixon, C. A., Irwin, P. G. J., Feb. 2020. Mapping the zonal structure of Titan's northern polar vortex. Icarus 337, 113441.

Sharkey, J., Teanby, N. A., Sylvestre, M., Mitchell, D. M., Seviour, W. J. M., Nixon, C. A., Irwin, P. G. J., Jan. 2021. Potential vorticity structure of Titan's polar vortices from Cassini CIRS observations. Icarus 354, 114030.

Shebanits, O., Wahlund, J.-E., Edberg, N. J. T., Crary, F. J., Wellbrock, A., Andrews, D. J., Vigren, E., Desai, R. T., Coates, A. J., Mandt, K. E., Waite, J. H., Oct. 2016. Ion and aerosol precursor densities in Titan's ionosphere: A multi-instrument case study. Journal Of Geophysical Research-Space Physics 121 (1), 10–.

Sittler, E.-C., Ali, A., Cooper, J.-F., Hartle, R.-E., Johnson, R.-E., Coates, A.-J., Young, D.-T., Nov. 2009. Heavy ion formation in Titan's ionosphere: Magnetospheric introduction of free oxygen and a source of Titan's aerosols? Planet. Space Sci. 57, 1547–1557.

Steffens, B. L., Nixon, C. A., Sung, K., Irwin, P. G. J., Lombardo, N. A., Pereira, E., Mar. 2022. New Constraints on Titan's Stratospheric n-Butane Abundance. 3 (3), 59.

Strobel, D., 1974. The photochemistry of hydrocarbons in the atmosphere of Titan. Icarus 21, 466–470.

Strobel, D., 2010. Molecular hydrogen in Titan's atmosphere: Implications of the measured tropospheric and thermospheric mole fractions. Icarus 208, 878–886.

Strobel, D. F., 2006. Gravitational tidal waves in Titan's upper atmosphere. Icarus 182, 251–258.

Strobel, D. F., Apr. 2022. Molecular hydrogen in the upper atmospheres of Saturn and Titan. 376, 114876.

Sylvestre, M., Teanby, N. A., Vinatier, S., Lebonnois, S., Irwin, P. G. J., 2018. Seasonal evolution of C_2N_2, C_3H_4, and C_4H_2 abundances in Titan's lower stratosphere. Astron. Astrophys. 609, A64.

Tazaki, R., May 2021. Analytic expressions for geometric cross-sections of fractal dust aggregates, 1–11.

Teanby, N. A., Bézard, B., Vinatier, S., Sylvestre, M., Nixon, C. A., Irwin, P. G. J., de Kok, R. J., Calcutt, S. B., Flasar, F. M., 2017. The formation and evolution of titan's winter polar vortex. Nature Comms. 8 (1), 1586.

Teanby, N. A., Cordiner, M. A., Nixon, C. A., Irwin, P. G. J., Hörst, S. M., Sylvestre, M., Serigano, J., Thelen, A. E., Richards, A. M. S., Charnley, S. B., Jun. 2018. The Origin of Titan's External Oxygen: Further Constraints from ALMA Upper Limits on CS and CH_2NH. 155 (6), 251.

Teanby, N. A., de Kok, R., Irwin, P. G. J., Osprey, S., Vinatier, S., Gierasch, P. J., Read, P. L., Flasar, F. M., Conrath, B. J., Achterberg, R. K., Bezard, B., Nixon, C. A., Calcutt, S. B., 2008. Titan's winter polar vortex structure revealed by chemical tracers. J. Geophys. Res. 113, E12003.

Teanby, N. A., Irwin, P. G. J., de Kok, R., 2010a. Compositional evidence for Titan's stratospheric tilt. Plan. & Space Sci. 58, 792–800.

Teanby, N. A., Irwin, P. G. J., de Kok, R., Nixon, C. A., 2009. Dynamical implications of seasonal and spatial variations in Titan's stratospheric composition. Phil. Trans. R. Soc. Lond. A 367, 697–711.

Teanby, N. A., Irwin, P. G. J., de Kok, R., Nixon, C. A., 2010b. Mapping Titan's HCN in the far infra-red: implications for photochemistry. Faraday Discussions 147, 51–64.

Teanby, N. A., Irwin, P. G. J., de Kok, R., Nixon, C. A., 2010c. Seasonal changes in Titan's polar trace gas abundance observed by Cassini. Astrophys. J. Lett. 724, L84–L89.

Teanby, N. A., Irwin, P. G. J., de Kok, R., Nixon, C. A., Coustenis, A., Bézard, B., Calcutt, S. B., Bowles, N. E., Flasar, F. M., Fletcher, L., Howett, C., Taylor, F. W., 2006. Latitudinal variations of HCN, HC_3N, and C_2N_2 in Titan's stratosphere derived from Cassini CIRS data. Icarus 181, 243–255.

Teanby, N. A., Irwin, P. G. J., Nixon, C. A., Courtin, R., Swinyard, B. M., Moreno, R., Lellouch, E., Rengel, M., Hartogh, P., 2013. Constraints on Titan's middle atmosphere ammonia abundance from Herschel/SPIRE sub-millimetre spectra. Plan. & Space Sci. 75, 136–147.

Teanby, N. A., Irwin, P. G. J., Nixon, C. A., de Kok, R., Vinatier, S., Coustenis, A., Sefton-Nash, E., Calcutt, S. B., Flasar, F. M., 2012. Active upper-atmosphere chemistry and dynamics from polar circulation reversal on Titan. Nature 491, 732–735.

Teanby, N. A., Sylvestre, M., Sharkey, J., Nixon, C. A., Vinatier, S., Irwin, P. G. J., 2019. Seasonal Evolution of Titan's Stratosphere During the Cassini Mission. Geophys. Res. Lett. 46 (6), 3079–3089.

Thelen, A. E., Cordiner, M. A., Nixon, C. A., Vuitton, V., Kisiel, Z., Charnley, S. B., Palmer, M. Y., Teanby, N. A., Irwin, P. G. J., Nov. 2020. Detection of CH_3C_3N in Titan&'s Atmosphere. 903 (1), L22.

Thelen, A. E., Nixon, C. A., Chanover, N. J., Cordiner, M. A., Molter, E. M., Teanby, N. A., Irwin, P. G. J., Serigano, J., Charnley, S. B., 2019. Abundance measurements of Titan's stratospheric HCN, HC_3N, C_3H_4, and CH_3CN from ALMA observations. Icarus 319, 417–432.

Thelen, A. E., Nixon, C. A., Cosentino, R. G., Cordiner, M. A., Teanby, N. A., Newman, C. E., Irwin, P. G. J., Charnley, S. B., 2022. Variability in Titan's Mesospheric HCN and Temperature Structure as Observed by ALMA. Plan. Sci. J. 3 (6), 146.

Thissen, R., Vuitton, V., Lavvas, P., Lemaire, J., Dehon, C., Dutuit, O., Smith, M. A., Turchini, S., Catone, D., Yelle, R. V., Pernot, P., Somogyi, Á., Coreno, M., 2009. Laboratory Studies of Molecular Growth in the Titan Ionosphere†. J. Phys. Chem. A 113 (42), 11211–11220.

Tigrine, S., Carrasco, N., Bozanic, D. K., Garcia, G. A., Nahon, L., Nov. 2018. FUV Photoionization of Titan Atmospheric Aerosols. The Astrophysical Journal 867 (2), 164.

Tobie, G., Lunine, J., Sotin, C., 2006. Episodic outgassing as the origin of atmospheric methane on Titan. Nature 440, 61–64.

Tobie, G., Teanby, N. A., Coustenis, A., Jaumann, R., Raulin, F., Schmidt, J., Carrasco, N., Coates, A. J., Cordier, D., De Kok, R., Geppert, W. D., Lebreton, J. P., Lefevre, A., Livengood, T. A., Mandt, K. E., Mitri, G., Nimmo, F., Nixon, C. A., Norman, L., Pappalardo, R. T., Postberg, F., Rodriguez, S., Schulze-Makuch, D., Soderblom, J. M., Solomonidou, A., Stephan, K., Stofan, E. R., Turtle, E. P., Wagner, R. J., West, R. A., Westlake, J. H., 2014. Science goals and mission concept for the future exploration of Titan and Enceladus. Plan. & Space Sci. 104, 59–77.

Tomasko, M., Buchhauser, D., Bushroe, M., Dafoe, L., Doose, L., Eibl, A., Fellows, C., McFarlane, E., Prout, G., Pringle, M., et al., 2003. The descent imager/spectral radiometer (disr) experiment on the huygens entry probe of titan. The Cassini-Huygens Mission: Overview, Objectives and Huygens Instrumentarium Volume 1, 469–551.

Tomasko, M., Doose, L., Engel, S., Dafoe, L., West, R., Lemmon, M., Karkoschka, E., See, C., 2008. A model of Titan's aerosols based on measurements made inside the atmosphere. Planet. Space Sci. 56, 669–707.

Tomasko, M., West, R., 2009. Aerosols in Titan's Atmosphere. In: Brown, R.H. andLebreton, J.-P., Waite, J. H. (Eds.), Titan from Cassini-Huygens. pp. 297–321.

Vigren, E., Galand, M., Shebanits, O., Wahlund, J.-E., Geppert, W. D., Lavvas, P., Vuitton, V., Yelle, R. V., Apr. 2014. Increasing positive ion number densities below the peak of ion-electron pair production in Titan's ionosphere. The Astrophysical Journal 786 (1), 69.

Vigren, E., Galand, M., Yelle, R., Cui, J., Wahlund, J.-E., \AAgren, K., Lavvas, P., Müller-Wodarg, I., Strobel, D., Vuitton, V., Bazin, A., 2013. On the thermal electron balance in Titan's sunlit upper atmosphere. Icarus 223, 234–251.

Vinatier, S., Bézard, B., de Kok, R., Anderson, C., Samuelson, R., Nixon, C., Mamoutkine, A., Carlson, R., Jennings, D., Guandique, E., Bjoraker, G., Flasar, F., Kunde, V., 2010a. Analysis of Cassini/CIRS limb spectra of Titan acquired during the nominal mission II: Aerosol extinction profiles in the 600-1420 cm-1 spectral range. Icarus 210, 852–866.

Vinatier, S., Bézard, B., Lebonnois, S., Teanby, N. A., Achterberg, R. K., Gorius, N., Mamoutkine, A., Guandique, E., Jolly, A., Jennings, D. E., Flasar, F. M., 2015. Seasonal variations in Titan's middle atmosphere during the northern spring derived from Cassini/CIRS observations. Icarus 250, 95–115.

Vinatier, S., Bézard, B., Nixon, C. A., Mamoutkine, A., Carlson, R. C., Jennings, D. E., Guandique, E. A., Teanby, N. A., Bjoraker, G. L., Flasar, F. M., Kunde, V. G., 2010b. Analysis of Cassini/CIRS limb spectra of Titan acquired during the nominal mission I. hydrocarbons, nitriles and CO_2 vertical mixing ratio profiles. Icarus 205, 559–570.

Vinatier, S., Mathé, C., Bézard, B., Vatant d'Ollone, J., Lebonnois, S., Dauphin, C., Flasar, F. M., Achterberg, R. K., Seignovert, B., Sylvestre, M., Teanby, N. A., Gorius, N., Mamoutkine, A., Guandique, E., Jennings, D. E., 2020. Temperature and chemical species distributions in the middle atmosphere observed during Titan's late northern spring to early summer. Astron. Astrophys. 641, A116.

Vinatier, S., Rannou, P., Anderson, C., Bézard, B., de Kok, R., Samuelson, R., 2012. Optical constants of Titan's stratospheric aerosols in the 70-1500 cm-1 spectral range constrained by Cassini/CIRS observations. Icarus 219, 5–12.

Vinatier, S., Schmitt, B., Bézard, B., Rannou, P., Dauphin, C., de Kok, R., Jennings, D. E., Flasar, F. M., 2018. Study of Titan's fall southern stratospheric polar cloud composition with Cassini/CIRS: Detection of benzene ice. Icarus 310, 89–104.

Vuitton, V., Doussin, J.-F., Bénilan, Y., Raulin, F., Gazeau, M.-C., 2006a. Experimental and theoretical study of hydrocarbon photochemistry applied to Titan stratosphere. Icarus 185, 287–300.

Vuitton, V., Lavvas, P., Yelle, R., Galand, M., Wellbrock, A., Lewis, G., Coates, A., Wahlund, J.-E., 2009. Negative ion chemistry in Titan's upper atmosphere. Planet. Space Sci. 57, 1558–1572.

Vuitton, V., Yelle, R., Anicich, V., 2006b. The nitrogen chemistry of Titan's upper atmosphere revealed. Astrophys. J. 647 (2), L175–L178.

Vuitton, V., Yelle, R., Klippenstein, S., Hörst, S., Lavvas, P., 2019. Simulating the density of organic species in the atmosphere of Titan with a coupled ion-neutral photochemical model. Icarus 324, 120–197.

Vuitton, V., Yelle, R., McEwan, M., 2007. Ion chemistry and N-containing molecules in Titan's upper atmosphere. Icarus 191, 722–742.

Wahlund, J.-E., Galand, M., Müller-Wodarg, I., Cui, J., Yelle, R., Crary, F., Mandt, K., Magee, B., Waite Jr., J., Young, D., Coates, A., Garnier, P., \AAgren, K., André, M., Eriksson, A., Cravens, T., Vuitton, V., Gurnett, D., Kurth, W., 2009. On the amount of heavy molecular ions in Titan's ionosphere. Planet. Space Sci. 57, 1857–1865.

Waite, J., Young, D., Cravens, T., Coates, A., Crary, F., Magee, B., Westlake, J., 2007. The process of tholin formation in Titan's upper atmosphere. Science 316, 870–875.

Waite, J.-H., Cravens, T.-E., Ip, W.-H., Kasprzak, W.-T., Luhmann, J.-G., McNutt, R.-L., Niemann, H.-B., Yelle, R.-V., Mueller-Wodarg, I., Ledvina, S.-A., Scherer, S., Feb. 2005. Oxygen Ions Observed Near Saturn's A Ring. Science 307, 1260–1262.

Wellbrock, A., Coates, A., Jones, G., Lewis, G., Waite, J., 2013. Cassini CAPS-ELS observations of negative ions in Titan's ionosphere: Trends of density with altitude. Geophys. Res. Lett. 40, 4481–4485.

Wellbrock, A., Coates, A. J., Jones, G. H., Vuitton, V., Lavvas, P., Desai, R. T., Waite, J. H., Dec. 2019. Heavy negative ion growth in Titan's polar winter. Monthly Notices of the Royal Astronomical Society 490 (2), 2254–2261.

West, R., Lavvas, P., Anderson, C., Imanaka, H., 2014. Titan's haze. In: Titan: Interior, Surface, Atmosphere and Space Environment. Cambridge University Press, pp. 285–321.

West, R.-A., Balloch, J., Dumont, P., Lavvas, P., Lorenz, R., Rannou, P., Ray, T., Turtle, E.-P., Mar. 2011. The evolution of Titan's detached haze layer near equinox in 2009. Geophys. Res. Lett. 38, L06204.

West, R. A., Seignovert, B. t., Rannou, P., Dumont, P., Turtle, E. P., Perry, J., Roy, M., Ovanessian, A., Jun. 2018. The seasonal cycle of Titan's detached haze. Nature Astronomy 2, 495–500.

Wong, M. H., Mahaffy, P. R., Atreya, S. K., Niemann, H. B., Owen, T. C., Sep. 2004. Updated Galileo probe mass spectrometer measurements of carbon, oxygen, nitrogen, and sulfur on Jupiter. 171 (1), 153–170.

Yelle, R., Strobel, D., Lellouch, E., Gautier, D., 1997. Engineering models for titan's atmosphere. Huygens: Science, Payload and Mission 1177, 243–256.

Yelle, R. V., Koskinen, T., Palmer, M., 2021. Titan occultations of orion's belt observed with cassini/uvis. Icarus 368, 114587.

Yu, X., Hörst, S. M., He, C., McGuiggan, P., Kristiansen, K., Zhang, X., Dec. 2020. Surface Energy of the Titan Aerosol Analog "Tholin". The Astrophysical Journal 905 (2), 88.